Journal of Medicinal Chemistry

Article

pubs.acs.org/jmc

Studies on the ATP Binding Site of Fyn Kinase for the Identification of New Inhibitors and Their Evaluation as Potential Agents against Tauopathies and Tumors

Cristina Tintori,[†] Giuseppina La Sala,[†] Giulia Vignaroli,[†] Lorenzo Botta,[†] Anna Lucia Fallacara,[†,‡] Federico Falchi,[†,+] Marco Radi,[†,¶] Claudio Zamperini,[†] Elena Dreassi,[†] Lucia Dello Iacono,[†] Donata Orioli,[§] Giuseppe Biamonti,[§] Mirko Garbelli,[§] Andrea Lossani,[§] Francesca Gasparrini,[‡,∥] Tiziano Tuccinardi,[⊥] Ilaria Laurenzana,[#] Adriano Angelucci,[▽] Giovanni Maga,[§] Silvia Schenone,*[,○] Chiara Brullo,[○] Francesca Musumeci,[○] Andrea Desogus,[○] Emmanuele Crespan,*[,§] and Maurizio Botta[†,◆]

[†]Dipartimento Biotecnologie, Chimica e Farmacia, Università degli Studi di Siena, Via A. De Gasperi 2, I-53100 Siena, Italy

[‡]Dipartimento di Chimica e Tecnologie del Farmaco, Università La Sapienza, Piazzale Aldo Moro 5, I-00185 Roma, Italy

[§]Istituto di Genetica Molecolare, IGM-CNR, Via Abbiategrasso 207, I-27100 Pavia, Italy

[∥]Dipartimento di Medicina Molecolare, Sapienza Università di Roma, Piazzale Aldo Moro 5, 00185 Roma, Italy

[⊥]Dipartimento di Farmacia, Università di Pisa, Via Bonanno 6, 56126 Pisa, Italy

[#]Laboratory of Preclinical and Translational Research, IRCCS-Centro di Riferimento Oncologico Basilicata (CROB), Via Padre Pio 1, Rionero in Vulture 85028 Potenza Italy

[▽]Dipartimento di Scienze Cliniche Applicate e Biotecnologiche, Università dell'Aquila, Via Vetoio, 67100 Coppito, L'Aquila, Italy

[○]Dipartimento di Farmacia, Università di Genova, Viale Benedetto XV 3, I-16132 Genova, Italy

[◆]Biotechnology College of Science and Technology, Temple University, Biolife Science Building, Suite 333, 1900 N 12th Street, Philadelphia, Pennsylvania 19122, United States

Supporting Information

ABSTRACT: Fyn is a member of the Src-family of nonreceptor protein−tyrosine kinases. Its abnormal activity has been shown to be related to various human cancers as well as to severe pathologies, such as Alzheimer's and Parkinson's diseases. Herein, a structure-based drug design protocol was employed aimed at identifying novel Fyn inhibitors. Two hits from commercial sources (**1**, **2**) were found active against Fyn with K_i of about 2 μM, while derivative **4a**, derived from our internal library, showed a K_i of 0.9 μM. A hit-to-lead optimization effort was then initiated on derivative **4a** to improve its potency. Slightly modifications rapidly determine an increase in the binding affinity, with the best inhibitors **4c** and **4d** having K_is of 70 and 95 nM, respectively. Both compounds were found able to inhibit the phosphorylation of the protein Tau in an Alzheimer's model cell line and showed antiproliferative activities against different cancer cell lines.

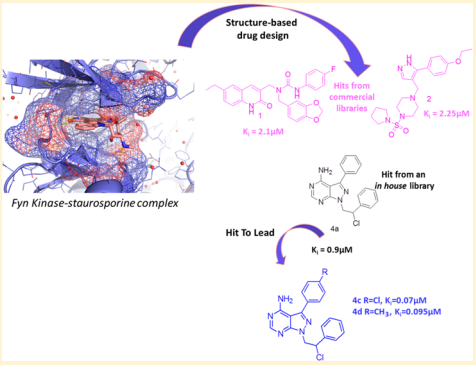

INTRODUCTION

Fyn is a nonreceptor tyrosine kinase belonging to the Src family kinases (SFKs).[1] The nine members of this family are grouped into subclasses: the SrcA subfamily which includes Src, Yes, Fyn, and Fgr, the SrcB subfamily containing Lck, Hck, Blk, and Lyn, and finally Frk in its own subfamily. Fyn is a 59 kDa protein comprising 537 amino acids, encoded by the Fyn gene, located on chromosome 6q21. Three isoforms of Fyn are known: FynB mainly expressed in the brain, FynT expressed in hematopoietic cells (T-cells), and FynDelta7, which has been identified in peripheral blood mononuclear cells.[2] In vertebrates, SFKs share a similar structure that comprises six distinct functional domains: Src homology domain 4 (SH4), a unique domain, SH3 domain, SH2 domain, a catalytic domain (SH1), and a C-terminal regulatory region. SH4 domain is a region which contains signals for modification with fatty acids.[1] The unique domain is specific for each Src family protein and is suggested to be responsible for peculiar interactions with particular receptors and protein targets.[3] SH2 and SH3 domains are involved in interactions with other proteins which regulate the tyrosine kinase activity. The kinase domain,

Received: January 26, 2015
Published: April 29, 2015

DOI: 10.1021/acs.jmedchem.5b00140
J. Med. Chem. 2015, 58, 4590−4609

which catalyzes the transfer of the terminal phosphate group of the ATP to a tyrosine residue of a protein substrate, shows a typical bilobed structure formed by a small N-terminal domain, involved in the ATP binding, and a larger C-terminal lobe, which contains the activation loop (A-loop) characterized by a tyrosine residue that is autophosphorylated in the active form of the enzyme.[4] The A-loop consists of 28 residues positioned between two conserved tripeptide motifs, DFG (Asp-Phe-Gly) and APE (Ala-Pro-Glu).[5] Besides sharing the same structure, the SFKs are also characterized by a common regulatory mechanism. In fact, the activation or inhibition of kinase activity depends on intramolecular interactions between SH2 and SH3 with the kinase domain and on phosphorylation/dephosphorylation of two critical tyrosines, the first situated in the A-loop and the second in the C-terminal region.[6] Fyn is able to interact with almost 300 different proteins and, through these interactions, participates in many cellular pathways, both in physiological and pathological situations.[7−9] Fyn is involved in the regulation of the immune system and in T-cell development and activation. It plays a crucial role in the development of the central nervous system (CNS), where it is implied in myelination and morphological differentiation associated with the formation of neurite in oligodendrocytes, synapse formation and regulation, oligodendrocyte differentiation, and memory formation.[10] Recent evidence suggest that Fyn hyperactivation/deregulation might contribute to Alzheimer's disease (AD) pathogenesis and other tauopathies. These diseases are characterized by the alteration in the amount or the structure of the Tau protein, a microtubule-associated protein that constitutes a fundamental component of the neurofibrillary tangles of AD.[11] In normal neurons, Tau is present in the cytoplasm in an unphosphorylated form. On the contrary, Tau results phosphorylated at multiple sites in AD. In particular, when associated with neurofibrillary tangles, Tau was found to be phosphorylated at its amino terminus residue Tyr18,[12] with Fyn being the sole kinase responsible for such event in AD. Mounting evidence suggest that the phosphorylation of Tyr18 is an early event in the pathophysiology of AD and leads to conformational changes in Tau, initiating its fibrillarization.[13] In addition, amyloid-beta (Aβ) was found to activate Fyn.[14] Moreover, overexpression of Fyn accelerates synapse loss and the onset of cognitive impairment in a transgenic AD mouse model, while inhibition of Fyn expression rescues synapse loss.[15] The AD therapeutic approaches currently in clinical trials are focused on Aβ clearance as well as on the inhibition of its production or aggregation. Therefore, due to its central role in Aβ signal transduction, Fyn represents a unique therapeutic target in AD.[9] On the other hand, Fyn overexpression has been shown to drive a morphologic transformation in normal cells, leading to tumor development. In fact Fyn is overexpressed in various cancers, including glioblastoma multiformae, squamous cell carcinoma of the head and neck, melanoma,[16] breast,[17] ovarian,[18] prostate,[19] and pancreatic cancer.[20] Recent studies have shown its involvement also in mesothelioma.[21] Lately, Singh and colleagues[22] demonstrated that Fyn kinase activity plays a role in the progression of chronic myeloid leukemia (CML) because it contributes to Bcr-Abl induced genomic instability, a feature of blast crisis CML.[23] The terminal, blast crisis phase of the disease remains a clinical challenge. Blast crisis CML is difficult to treat due to resistance to tyrosine kinase inhibitors, increased genomic instability, and acquired secondary mutations. Knockdown of Fyn leads to decreased cell growth and proliferation in vitro and in vivo. Moreover, it has been demonstrated that the complete loss of Fyn using genetic knockout models decreases the proliferation and clonogenic potential of cells transduced with Bcr-Abl, underscoring a dependency upon Fyn for Bcr-Abl mediated growth and clonogenicity. Additionally, using a cell line model of blast crisis CML, they discovered that overexpression of constitutively active Fyn caused increased aneuploidy and genomic alterations. Because of the involvement of Fyn in such disease, the search for Fyn inhibitors represents an expanding field of study. Herein, molecular modeling studies were combined with organic synthesis toward the development of novel Fyn kinase inhibitors. Both commercial libraries of small molecules and a family of pyrazolo[3,4-*d*]pyrimidines previously identified by our research group[24−32] were virtually screened within the ATP binding site of Fyn in order to select potential binding inhibitors. A hit-to-lead optimization process was then carried out on the most active Fyn inhibitor identified, resulting in the development of compounds active against Fyn with K_i values in the nanomolar range. Selected compounds showed an interesting antiproliferative activity profile against the human leukemia KU-812, the human breast cancer MDA-MD-231, and the human glioblastoma multiforme cell lines. Furthermore, they were found able to inhibit the Fyn-mediated phosphorylation of the protein Tau in an AD model cell line.

RESULTS AND DISCUSSION

Molecular Modeling and Enzymatic Activities on Isolated Fyn Kinase. A docking study was employed herein by means of the Gold software with the purpose of identifying novel ATP competitive Fyn kinase inhibitors. First, a library of commercially available compounds was analyzed to select the most promising binders of Fyn for biological investigation. Later, the same computational methodology was applied to screen an in-house library of pyrazolo[3,4-*d*]pyrimidines (consisting of ∼300 structurally characterized compounds with >98% purity). Once the accuracy of the computational procedure was checked by reproducing the experimental pose of the cocrystallized staurosporine as well as those of the known active ligands PP1 and PP2, the docking protocol was applied on the Asinex commercial database. A total of 703200 entries were evaluated in two consecutive pruning steps to optimize the balance between the quality of docking and the time required for calculations. Accordingly, the whole compound collection was first analyzed using the *Number of Run* parameter set to 10, thus allowing to speed up the process and to handle a large number of ligands in a reasonable computing time. The top 5000 scored hits were selected for a second run of docking calculations for which the *Number of Run* parameter was set to 100. The best ranked structures were visually inspected to evaluate the complementarity between each bound ligand and the protein surface in terms of size, shape, and interactions. Six compounds were finally selected and submitted to biological testing to evaluate their affinity toward Fyn in a cell-free assay. Results are listed in Table 1. Compounds **1** and **2** were identified as efficient Fyn inhibitors being endowed with K_i values of 2.1 and 2.25 μM, respectively. Figure 1 shows the binding mode of compounds **1** and **2** within the ATP binding site of Fyn kinase as predicted by docking analysis. The quinolinone scaffold of **1** forms two H-bonds with the backbone of Met 345, while the 1,3-benzodioxole ring is directed toward an hydrophobic cavity of the binding site, where it forms a H-bond with the nitrogen backbone of Asp408 and interacts with Val327, Ala407, and the aliphatic chain of

DOI: 10.1021/acs.jmedchem.5b00140
J. Med. Chem. 2015, 58, 4590−4609

Table 1. Code and Inhibitory Activities of Compounds Purchased from Asinex Vendor toward Isolated Fyn Kinase

compd code	Fyn (K_i) [μM]
ASN05112738 (**1**)	2.1
BAS01816455	NA[q]
SYN20066203	NA
SYN17915165	NA
ASN05112735	NA
SYN22890157 (**2**)	2.25

[q]NA means not active.

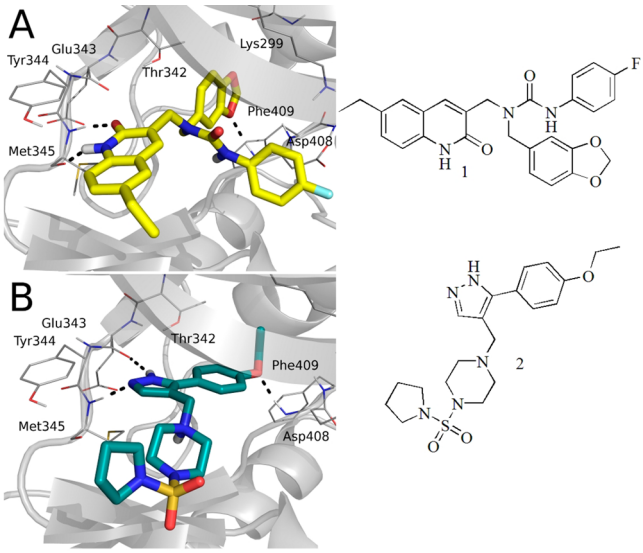

Figure 1. Binding mode of hit compounds (A) **1** (yellow stick) and (B) **2** (deep-teal) within the ATP binding site of Fyn kinase. For the sake of clarity, only a few key residues are visualized as stick representation, nonpolar hydrogen atoms are omitted, and hydrogen-bonding interactions are represented by black dashed lines.

Lys299. Remarkably, the binding mode identified for compound **1** is in perfect agreement to that found for a structurally closed Fyn inhibitor (published as compound VS3)[33] recently identified by us using a different computational approach. Interestingly, many analogues of compound **1** are available from Asinex and 19 of them have been previously selected as potential Fyn kinase inhibitors.[33] Within the virtual screening approach reported herein, such analogues showed docking dG ranging from −32 to −38 kJ/mol, comparable to that of compound **1** (dG = −37.48 kJ/mol), further confirming the potentiality of this chemical scaffold for the development of Fyn kinase inhibitors. With regard to compound **2**, the pyrazole ring makes hydrogen bonding with the NH of Met345 and the oxygen backbone of Glu343, both belonging to the hinge region. The ethoxyphenyl group fills the bottom side of the cavity where it establishes hydrophobic contacts with Val327, Ala407, and Lys299 as well as an H-bond with the NH backbone of Asp408. The pyrrolidine−sulfonyl−piperazine side chain is directed toward the solvent-exposed region of the binding site. A similarity search for compounds **1** and **2** within Scifinder showed that the latter has never been reported as a protein kinase inhibitor (there are no kinase ligands with a similarity score greater than 80).

On the other hand, an in-house library of pyrazolo[3,4-*d*]pyrimidines[24−32] was virtually screened against the active site of Fyn kinase using the docking protocol described before for the second run of calculations. From a structural point of view, these compounds are related to the Src inhibitors PP1 and PP2 but bear a different substitution pattern on the position 1, 3, 4, and 6 of the pyrazolo[3,4-*d*]pyrimidine nucleus. Seventeen compounds were selected for testing according to the predicted score values and the binding poses observed (Table 2). Among them, some derivatives (**3a−i**, **3p**) have been already reported by us as Bcr-Abl/Src inhibitors.[29−32] Other compounds have been never reported before. They include derivatives **3j**, **3k**, **3l**, and **3o**, which bear bulky thio-substituents or alkyl group on C6, the N1 styryl derivatives **3m** and **3n**, and the compound **4a**,

Table 2. Structure and Inhibitory Activities of Compounds 3a−p and 4a toward Isolated Fyn Kinase

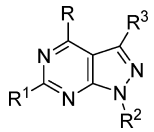

compd	R	R^1	R^2	R^3	Fyn (K_i) [μM]
3a	$NHCH_2CH_2C_6H_5$	SC_4H_9	CH_2-CHCl-C_6H_5	H	NA
3b	NHC_6H_4-*m*Cl	SC_4H_9	CH_2-CHCl-C_6H_5	H	1.4
3c	$NHCH_2CH_2C_6H_5$	*S*-cyclopentyl	CH_2-CHCl-C_6H_5	H	NA
3d	NHC_6H_4-*m*F	*S*-cyclopentyl	CH_2-CHCl-C_6H_5	H	NA
3e	NHC_6H_4-*m*Cl	*S*-cyclopentyl	CH_2-CHCl-C_6H_5	H	NA
3f	NHC_3H_7	SCH_2CH_2-4morpholino	CH_2-CHCl-C_6H_5	H	8.15
3g	$NHCH_2C_6H_4$-*p*F	SCH_2CH_2-4morpholino	CH_2-CHCl-C_6H_5	H	15.5
3h	$NHCH_2CH_2C_6H_5$	SCH_2CH_2-4morpholino	CH_2-CHCl-C_6H_5	H	NA
3i	NHC_6H_5	SCH_2CH_2-4morpholino	CH_2-CHCl-C_6H_5	H	7.5
3j	$NHCH_2C_6H_5$	*S*-CH(CH_3)C_2H_5	CH_2-CHCl-C_6H_5	H	NA
3k	$NHCH_2CH_2C_6H_5$	*S*-CH(CH_3)C_2H_5	CH_2-CHCl-C_6H_5	H	NA
3l	NHC_6H_4-*m*Cl	*S*-CH(CH_3)C_2H_5	CH_2-CHCl-C_6H_5	H	12.5
3m	$NHCH_2CH_2C_6H_4$-*m*Cl	SCH_3	CH═CH-C_6H_5	H	16
3n	$NHCH_2C_6H_5$	$NHCH_2CH_2OH$	CH═CH-C_6H_5	H	1.15
3o	$NHCH_2C_6H_5$	$CH_2C_6H_5$	CH_2-CHCl-C_6H_5	H	13
3p	$NHCH_2C_6H_5$	H	CH_2-CHCl-C_6H_5	H	3.5
4a	NH_2	H	CH_2-CHCl-C_6H_5	C_6H_5	0.9

DOI: 10.1021/acs.jmedchem.5b00140
J. Med. Chem. 2015, 58, 4590−4609

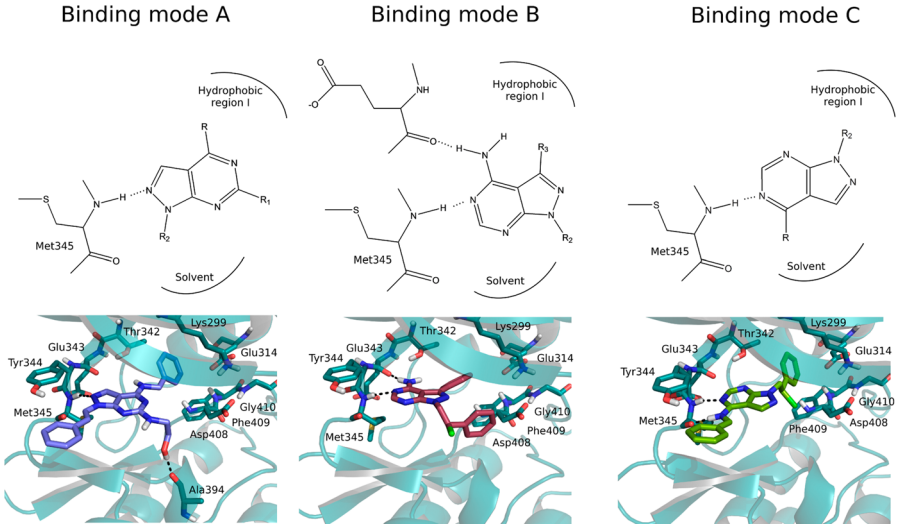

Figure 2. 2D and 3D graphical representation of the predicted binding modes of pyrazolo[3,4-*d*]pyrimidines **3a**–**p** and **4a**. Three different poses were detected, namely binding modes A, B, and C. Compounds **3n** (violet), **4a** (salmon), and **3p** (limon) are visualized within the ATP binding site of Fyn as representative of binding modes A, B, and C, respectively.

bearing a C3 phenyl ring and a C4 unsubstituted amino group. Three different binding modes emerged from docking studies. Compounds **3a**–**3o**, functionalized at positions 1, 4, and 6 and C3-unsubstituted, showed an interaction pattern similar to that previously found within the ATP binding site of c-Src (herein referred to as BM A, Figure 2).[28] The pyrazolo[3,4-*d*]pyrimidine core occupies the adenine region, the C4 substituent establishes hydrophobic interactions with Leu329, Phe409, Ile340, Phe311, Met318, and Leu411, (hydrophobic region I), while the N1 side chain is involved in van der Waals contacts with Tyr344, Met345, and Leu277 (hydrophobic region II). The C6 substituent is directed toward the external region though still involved in nonpolar contacts with Val285 and Lys299. Two hydrogen bond interactions were also found, one involving the C4 amino group and the side chain of Thr342 and the other between the N2 of the pyrazolo[3,4-*d*]pyrimidine nucleus and the backbone NH group of Met345. Conversely, the binding mode B (BM B, Figure 2) was identified for compound **4a** which brings a substituent at the C3 position while it is unsubstituted at C6. **4a** is a close analogue of PP1 and PP2, the first reported Fyn inhibitors.[34] Accordingly, its binding mode is consistent with that previously identified for PP1 and PP2 by crystallographic experiments and reproduced herein by docking studies (compare the BM B in Figure 2 with the binding mode of PP2 within the Fyn kinase active site visualized in Figure 3A).[35,36] In detail, the exocyclic amine makes an H-bond with the carbonyl backbone of Glu343, while the nitrogen at N5 position acts as H-bond acceptor in the interaction with Met345. The C3 phenyl group binds to the residues of hydrophobic region I through van der Waals interactions, while the N1 group is solvent exposed. Finally, compound **3p** which is unsubstituted at both C3 and C6 positions showed the binding mode C visualized in Figure 2. According to our prediction, the ligand binds the Met345 of the hinge region through two hydrogen bonds by means of the atom N5 and the exocyclic amino group at C4. Moreover, the N1 side chain is located within the hydrophobic pocket I formed by residues Leu329, Phe409, Ile340, Phe311, Met318, and Leu411 while the substituent at C4 interacts with Tyr344 and Leu277 of hydrophobic region II. Finally, as a result from

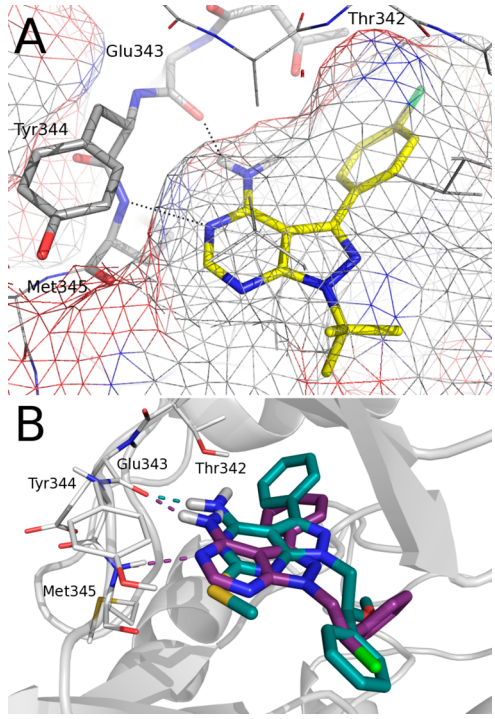

Figure 3. (A) Binding mode of PP2 (yellow) within the ATP binding pocket of Fyn kinase as predicted by docking. (B) Superimposition between **4a** (purple) and **6b** (teal) derived from docking studies. Pose of active compound **4a** coincides with that of the known PP2 inhibitor.

biological investigation on isolated Fyn kinase (Table 2), **3b**, **3n**, **3p**, and **4a** resulted in being the most active compounds, being endowed with K_i values of 1.4, 1.15, 3.5 μM and 0.9 μM, respectively. Derivatives **3f**, **3g**, **3i**, **3l**, **3m**, and **3o** exhibited moderate activity with K_i ranging from 7.5 to 16 μM. No activity was detected for the remaining compounds.

On the basis of this finding, a hit to lead optimization campaign was then initiated on compound **4a** to improve its potency. Nine analogues were synthesized (**4b**–**e**, **5a**–**e**) (Table 3). The C3 moiety was differently functionalized, while little modifications were carried out on the 2-chloro-2-

DOI: 10.1021/acs.jmedchem.5b00140
J. Med. Chem. 2015, 58, 4590–4609

Table 3. Structure and Inhibitory Activities of Compounds 4b−e, 5a−e, and 6a−b toward Isolated Fyn Kinase[a]

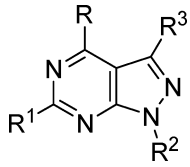

Cpd	R	R[1]	R[2]	R[3]	Fyn (K_i) [μM]	IC_{50}±SD [μM] (K562 cells)
4b	NH_2	H	CH_2-CHCl-C_6H_5	C_6H_4-*p*F	0.36	12.63±14.80
4c	NH_2	H	CH_2-CHCl-C_6H_5	C_6H_4-*p*Cl	0.07	0.56±0.01
4d	NH_2	H	CH_2-CHCl-C_6H_5	C_6H_4-*p*CH_3	0.095	0.30±0.06
4e	NH_2	H	CH_2-CHCl-C_6H_5	C_6H_4-*p*OCH_3	1.485	ND[b]
5a	NH_2	H	CH_2-$CHCH_3$-C_6H_5	C_6H_5	3.35	ND
5b	NH_2	H	CH_2-$CHCH_3$-C_6H_5	C_6H_4-*p*Cl	0.78	ND
5c	NH_2	H	CH_2-$CHCH_3$-C_6H_5	C_6H_4-*p*CH_3	0.995	ND
5d	NH_2	H	CH_2-$CHCH_3$-C_6H_5	C_6H_4-*p*$COCH_3$	>10	ND
5e	NH_2	H	CH_2-$CHCH_3$-C_6H_5	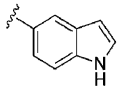	1.625	ND
6a	$NHCH_3$	SCH_3	$CH_2CH_2C_6H_5$	C_6H_5	>10	ND
6b	NH_2	SCH_3	$CH_2CH(OCH_3)$-C_6H_5	C_6H_5	>10	ND

[a]Antiproliferative activity of Fyn-targeting agents **4b−d** against the CML K562 cells is also reported. [b]ND = not determined.

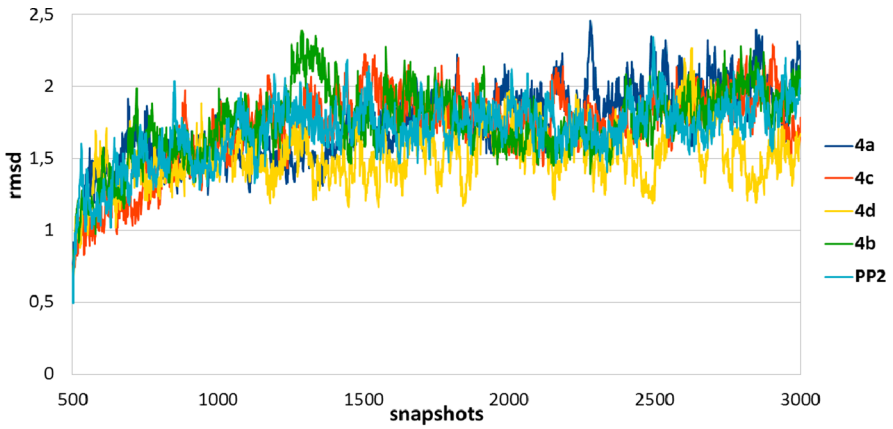

Figure 4

Figure 4. Time evolution of the RMSD values (calculated on α carbons) of the complexes between Fyn and compounds PP2, **4a−d** analyzed by MD simulations.

phenylethyl N1 side chain by replacing or removing the chlorine atom. Furthermore, with the aim of exploring the effect caused by the introduction of a S-methyl moiety at the C6 position of the C3-phenyl-substituted pyrazole[3,4-*d*]-pyrimidine core, derivatives **6a** and **6b**, previously synthesized by our group,[37] were added to this set of compounds. The 11 compounds were tested in a cell-free assay to evaluate their affinity toward isolated Fyn kinase.

As it can be appreciated from Table 3, derivatives **4c** and **4d** showed potent in vitro inhibitory effect against Fyn, with K_i values in the nanomolar range (70 and 95 nM, respectively). These potencies were most likely evoked due to the contribution of a chlorine or methyl substituent in *para* position of the C3 phenyl ring (compare **4c** with **4a** and **4d** with **4a**).

Interesting activities were also found for compounds **4b**, **5b**, and **5c**, which exhibited submicromolar affinities (0.36, 0.78 μM and 0.995 μM, respectively). As a general trend, the substitution of chlorine by methyl in the N1 side chain led to a considerable reduction of the affinity with about 10-fold decreased activities (compare **5a** with **4a**, **5b** with **4c**, and **5c** with **4d**). No activity was found for compounds **6a** and **6b** bearing a methylthio group at the C6 position. To rationalize such biological data, docking studies were carried out on the second generation series of compounds (**4b−d**, **5a−e**, **6a**,**b**), and the resulting binding modes were compared with that previously identified for the starting hit **4a** (BM B in Figure 2). All studied compounds adopted a pose in line with that of **4a**, with the exception of the inactive derivatives **5d** and **6a**,**b**. With regard to compounds **6a**,**b**, despite they maintained an orientation similar to that of **4a** within the ATP binding site of Fyn, the presence of the substitution in C6 position does not allow the ligands to properly interact with the residues of the hinge region moving away the pyrazolo-pyrimidine scaffold from such amino acids. As a consequence, the hydrogen bond between N5 and Met345 is lost in compound **6b** (Figure 3B), while both polar contacts with the hinge region were missing in the complex between Fyn and **6a**. Vice versa, the optimization

DOI: 10.1021/acs.jmedchem.5b00140
J. Med. Chem. 2015, 58, 4590−4609

of the van der Waals contacts within the hydrophobic region I of ligands **4b**, **4c**, **4d**, **5b**, and **5c**, due to the introduction of an hydrophobic substituent such as F, Cl, or CH_3 at the *para* position of the C3 phenyl ring, rapidly determines an increase in the binding affinity.

To assess the stability of the complexes and to gain further insight into the ligand−protein interactions, molecular dynamics (MD) simulations were carried out starting from the geometry obtained by docking. The complexes between Fyn and derivatives **4a**, **4b**, **4c**, and **4d** were selected as the training set. Furthermore, the same computational protocol was applied on the complex between Fyn and the known ligand PP2 for comparison purposes. Each simulation was carried out for a total of 12 ns. Figure 4 shows the time evolution of the root-mean-square deviation (RMSD) calculated on all heavy atoms during the time of simulation with respect to the starting structures. For each analyzed complex, we observed an initial increase due to the equilibration of the system, followed by a stabilization of the RMSD value around 1.9, 1.80, 1.82, 1.57, and 1.77 Å with ligands **4a**, **4b**, **4c**, **4d** and PP2, respectively (RMSD average value was calculated from frame 1500 to 3000). The last 6 ns of all simulations were regarded as stable and used to extract 150 evenly spaced-out snapshots from each trajectory. Molecular mechanics Poisson−Boltzmann/generalized Born surface area (MM-PB/GBSA) approaches were then applied to estimate the free energy of binding between protein and ligands. The computed values are reported in Table 4. It must be noted that a better correlation between computed binding energies and experimental free energies of binding for congeneric compounds **4a−d** was observed for the GB method for which the higher Pearson's correlation coefficient was determined (r^2 of 0.83 vs 0.47). Taking also into consideration that GB calculations are less time-expensive than PB calculations, the former resulted as being the best choice for the future optimization of the pyrazolo[3,4-*d*]pyrimidines as Fyn kinase inhibitors. Next, to go into the details of the interactions which play a pivotal role in the ligand−protein recognition process, a post processing analysis was conducted on the complexes including hydrogen-bond analysis and monitoring of the root-mean-square fluctuations of the binding site residues.

Table 4. Binding Free Energies of the Complexes between Fyn and 4a−d Inhibitors Computed with Both MM-GBSA and MM-PBSA Approaches

compd	ΔG_{bind} MMGBSA	ΔG_{bind} MMPBSA
4a	−35.07 ± 2.25	−27.45 ± 3.63
4b	−38.21 ± 2.75	−29.81 ± 3.64
4c	−40.51 ± 2.63	−34.98 ± 3.55
4d	−38.36 ± 3.26	−29.73 ± 3.96

H-Bond Analysis. Hydrogen-bonding interactions between ligands and receptor as well as between the main residues of the active site were determined and listed in Table 5 together with their occupancy in the investigated time period. A weak hydrogen bond (occupancy of about 30%) was found between the nitrogen at position 5 (N5) of each ligand and the NH backbone of Met345. Conversely, the carbonyl backbone of Glu343 established a stable hydrogen-bond contact (occupancy higher than 60%) with the ligand exocyclic amine (N4). As a consequence of this hydrogen bond, the intermolecular interaction between the Thr342 side chain and the carbonyl backbone of Glu343 is weakened. This effect is particularly pronounced for the most active inhibitors **4c** and **4d** for which the Thr342−Glu343 polar contact is totally lost as well as for PP2 ligand. Furthermore, no interaction was detected between N4 and the Thr342 side chain, and this could be due to the fact that the "gatekeeper" residue is stabilized in its position by favorable interactions with Ala297 (Table 5). On the other hand, it has been previously demonstrated that the active conformation of Fyn is overexpressed in pathological conditions.[10,16,17,19−23] In addition, the main interactions for the stabilization of this conformation have been identified by means of crystallography studies. Among them, the electrostatic network between the catalytic Lys299 and the Glu314 belonging to the αC helix stabilizes the receptor in its active conformation. Taking into account this information, we also monitored the Lys299−Glu314 hydrogen-bonding interactions during the MD simulations (Table 6). As a result, the salt bridge was rather stable for all complexes, suggesting the ability for the studied inhibitors of interacting and stabilizing the Fyn active conformation. Furthermore, a larger network of interactions emerged for residues Lys299 and Glu314 in complexes **4b−d**. In detail, in such systems Lys299 is also involved in a salt bridge with the side chain of Asp408 and, at the same time, the Glu314 participates in an H-bond with the NH backbone of Phe409. Such a pool of interactions further contributes to the stabilization of the complexes in the active conformation.

Table 6. Permanence of the Hydrogen Bonds Involving Residues Lys299, Glu314, Asp408, and Phe409 during the Time of Simulation

compd	Lys299−Glu314	Lys299−Asp408	Glu314−Phe409
4a	75.5		12.72
4b	128.33	55.89	14.77
4c	138.23	90.35	10.65
4d	130.36	72.63	75.92
PP2	98.94		

RMSF. Root-mean-square fluctuations (RMSFs) of the α-carbons of each residue were calculated during the production phase of MD simulation of the analyzed complexes, and results were compared with those coming from a MD simulation of Fyn kinase in its apo form (Figure 5). It is interesting to note that some regions of the kinase domain which directly interact

Table 5. Hydrogen Bonds Occupancy for 4a−d and PP2 Ligands in Complex with Fyn

compd	Glu343(O) N4 (%)	Met345(NH) N5 (%)	Thr342(OGH) Ala297(O) (%)	Thr342(OGH) Glu343(O) (%)	Thr342(NH) Ala297(O) (%)
4a	67.4	33.3	54	5.7	88.3
4b	62	32.9	20	24.18	85.5
4c	76	32.8	53.2		85.7
4d	77.1	30.6	51.5		89.4
PP2	68.8	34.6	47.6		74.7

DOI: 10.1021/acs.jmedchem.5b00140
J. Med. Chem. 2015, 58, 4590−4609

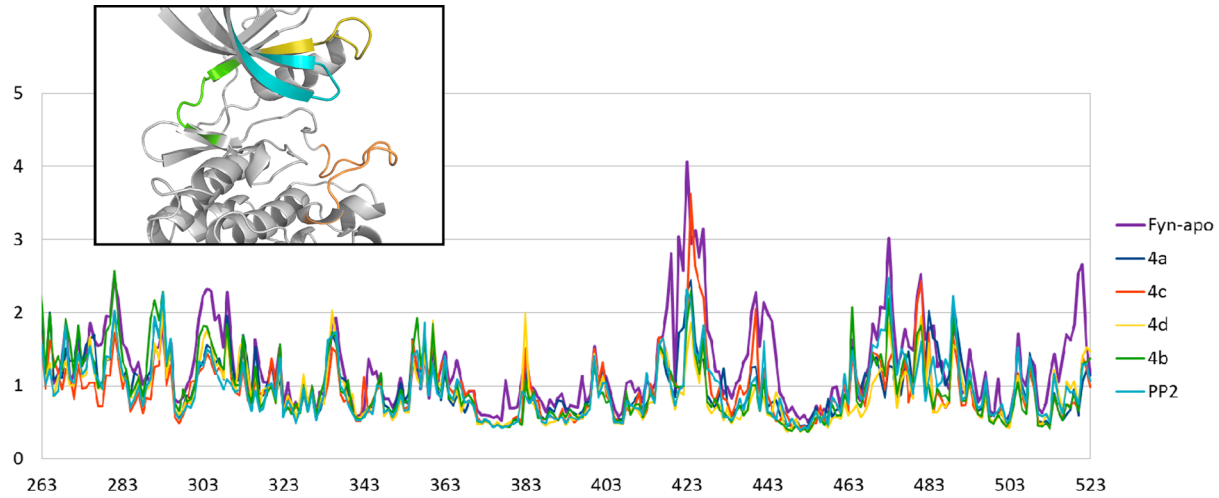

Figure 5. RMSF value of each residue calculated from the MD simulations on all the studied complexes. The number of residues is reported in abscissa while the RMSF expressed in Å is reported in the ordinate. The bottom graph shows the regions important for our study: the G-loop (cyan), the portion between the β3 strand and the αC helix (yellow), the hinge region (green), and the A-loop (orange).

Scheme 1. Synthesis of Compounds 3j−m and 3q−s[a]

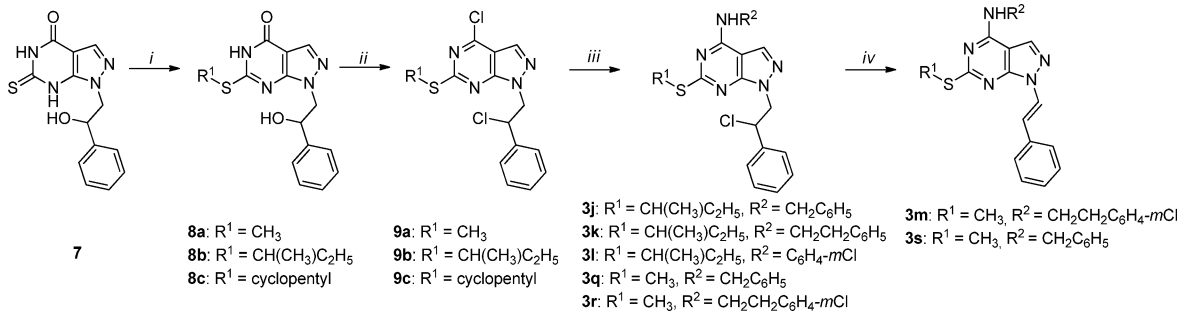

[a]Reagents and conditions: (i) method A, CH_3I, anhyd THF, reflux, 12 h (for **8a**); method B, R^1-Br, K_2CO_3, anhyd DMF, rt, 24 h (for **8b** and **8c**); (ii) $POCl_3$/DMF, $CHCl_3$, reflux, 4−8 h; (iii) method A, R^2NH_2, anhyd toluene, rt, 48 h (for **3j**, **3k**, **3q**, and **3r**); method B, R^2NH_2, EtOH, reflux, 5 h (for **3l**); (iv) 4N NaOH, EtOH, reflux, 5 h.

with compounds **4a−d** and PP2 showed a lower flexibility in complexes with respect to the free receptor. In particular, this corresponds to the loop between β3 strand and αC helix (residues from 300 to 310 highlighted in yellow in Figure 5), the A-loop (residues from 416 to 431 highlighted in orange in Figure 5), and the glycine rich loop or G-loop (residues from 274 to 286 in cyan blue in Figure 5). Focusing on G-loop, the RMSFs values obtained for complexes **4a−d** were in line with the experimental activities. Indeed, lower fluctuations were found with the most active inhibitor **4c**, suggesting that the stabilization of the G-loop could plays a key role in determining the potency of a ligand against Fyn.

Chemistry. The synthesis of compounds **3j−n** was performed starting from 1-(2-hydroxy-2-phenylethyl)-6-thioxo-1,5,6,7-tetrahydro-4*H*-pyrazolo[3,4-*d*]pyrimidin-4-one **7**, previously reported by us.[38] Alkylation of the C6 thiocarbonyl group with the suitable alkyl bromide in anhydrous *N*,*N*-dimethylformamide (DMF) at room temperature afforded the 6-alkylthio derivatives **8a−c**, in turn treated with the Vilsmeier complex ($POCl_3$/DMF, 1:1) in $CHCl_3$ to obtain the dichloro-derivatives **9a−c**. Finally, reaction with an excess of the appropriate amines in toluene at room temperature afforded compounds **3j**, **3k**, **3r**, and **3q** in good yields. Differently, compound **3l** was obtained reacting **9b** with *m*-chloroaniline in absolute ethanol at reflux for 5 h. Compounds **3m** and **3s** have been obtained by treatment of **3q** and **3r** with a 4N NaOH solution at reflux for 5 h (Scheme 1). Oxidation of compound **3s** with *meta*-chloroperoxybenzoic acid (*m*CPBA) in $CHCl_3$ gave the 6-methylsulfonyl derivative **10**. Finally, **3n** was obtained by nucleophilic substitution of the methylsulfonyl group with 2-aminoethanol in dimethyl sulfoxide (DMSO) and butan-1-ol at 90 °C for 12 h in good yield (Scheme 2). Compound **3o** was obtained starting from 2-hydrazino-1-phenylethanol **11**.[39] The synthesis of **12** and **13** was previously reported by us,[40] but in this study compound **12** was prepared through an alternative method that uses microwave irradiation,

Scheme 2. Synthesis of Compound 3n[a]

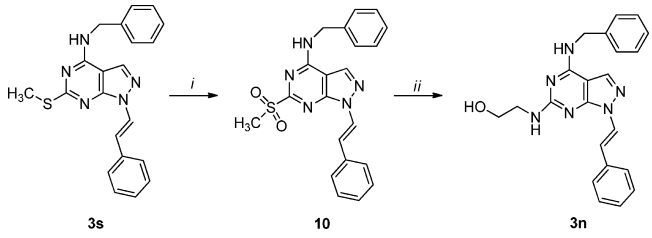

[a]Reagents and conditions: (i) mCPBA, $CHCl_3$, rt, 6 h; (ii) 2-aminoethanol, DMSO, butan-1-ol, 90 °C, 12 h.

DOI: 10.1021/acs.jmedchem.5b00140
J. Med. Chem. 2015, 58, 4590−4609

with the purpose of shortening the reaction times. 5-Amino-1-(2-hydroxy-2-phenylethyl)-1*H*-pyrazole-4-carboxamide **13** was treated with sodium ethoxide and methyl phenylacetate in absolute ethanol at reflux for 6 h to afford 6-benzyl-1-(2-hydroxy-2-phenylethyl)-1,5-dihydro-4*H*-pyrazolo[3,4-*d*]-pyrimidin-4-one **14**. This last was in turn chlorinated with the Vilsmeier complex in $CHCl_3$ at reflux for 12 h and gave the dichloro derivative **15**, that by reaction with benzylamine afforded **3o** (Scheme 3). The synthesis of 3-susbtituted

Scheme 3. Synthesis of Compound 3o[a]

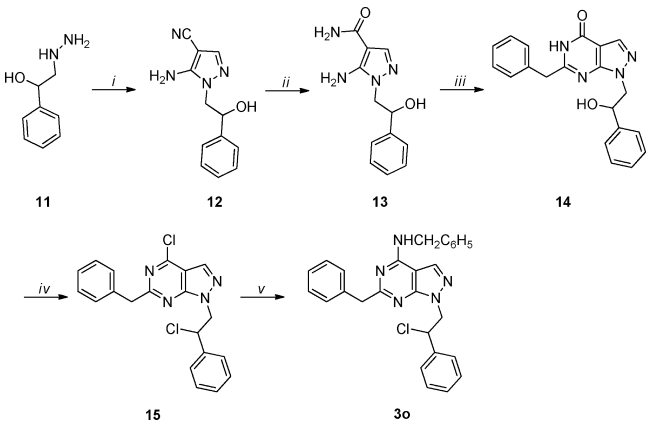

[a]Reagents and conditions: (i) ethoxymethylenemalononitrile, abs EtOH, MW, 60 °C, 100 W, 5 min; (ii) 2N NaOH, 95% EtOH, reflux, 3 h; (iii) methyl phenylacetate, EtONa, abs EtOH, reflux, 6 h; (iv) $POCl_3$/DMF, $CHCl_3$ reflux, 12 h; (v) benzylamine, anhyd toluene, rt, 48 h.

pyrazolo[3,4-*d*]pyrimidines **4a−e** was performed using a three-component one-pot synthesis.[41] Sodium hydride was added in small batches to a solution of malononitrile **16** in dry THF precooled at 0/5 °C; after 30 min, the suitable acyl chloride was added and the solution stirred at room temperature for 2−12 h. Then dimethylsulfate was added, and the solution was refluxed for 3−6 h. Finally, 2-hydrazino-1-phenylethanol **11** dissolved in dry THF was added and the reaction was refluxed for 4 h to afford intermediates **17a−e**, purified by flash chromatography. Compounds **17a−e** were suspended in formamide, and the mixture was heated at 190 °C for 3−4 h to afford the pyrazolo-pyrimidines **18a−e**, that were in turn reacted with thionyl chloride in dry CH_2Cl_2 at room temperature for 12 h under nitrogen atmosphere to give the final compounds **4a−e** (Scheme 4). We undertook a study, similar to that reported by Hanefeld et al.,[41] to compare the step-by-step synthesis to the one-pot procedure. This study was aimed at evaluating if the one-pot reaction was convenient in terms of time, cost, and green impact also for the synthesis of our derivatives bearing a N1 phenyletanolic chain. Compound **17d**, which was obtained with good yield in the one-pot synthesis, was selected for this study. In the step-by-step method, intermediates **19** and **20** were synthesized and isolated.[41] Finally, [methoxy(4 methylphenyl)methylene]-malononitrile **20** was reacted with 2-hydrazino-1-phenylethanol **11** in absolute ethanol at reflux for 8 h, giving the desired compound **17d** (Scheme 5). The yield of **17d** increases from

Scheme 5. Comparison between the Step-by-Step (A) and the One-Pot (B) Synthesis for Compound 17d[a]

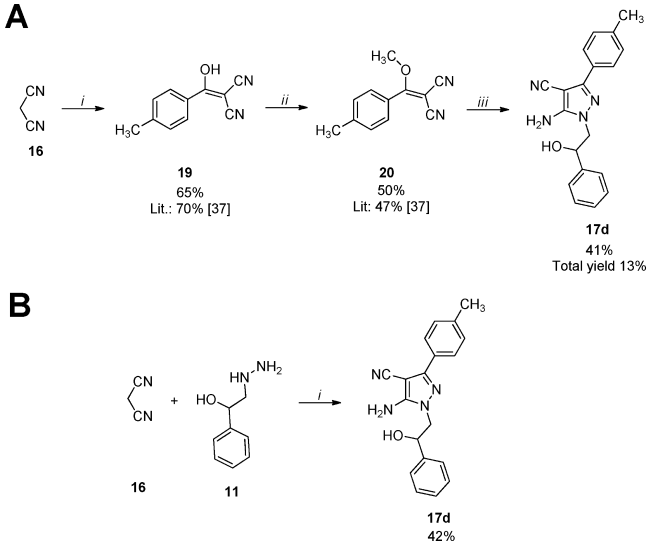

[a](A) Reagents and conditions: (i) NaH, *p*-tolylbenzoyl chloride, anhyd THF, rt, 3 h; (ii) Me_2SO_4, 1,4-dioxane, H_2O, 90 °C, 4 h; (iii) **11**, abs EtOH, reflux, 8 h. (B) Reagents and conditions: (i) (a) **16**, NaH, anhyd THF, 0/5 °C, 30 min; (b) *p*-tolyl benzoyl chloride, rt, 3.5 h; (c) Me_2SO_4, reflux, 3.5 h; (d) **11**, reflux, 4 h.

13% in the three-step procedure (Scheme 5A) to 42% in the one-step procedure (Scheme 5B). This allows saving of time and solvents. Synthesis of compounds **5a−e** was performed via

Scheme 4. Synthesis of Compounds 4a−e[a]

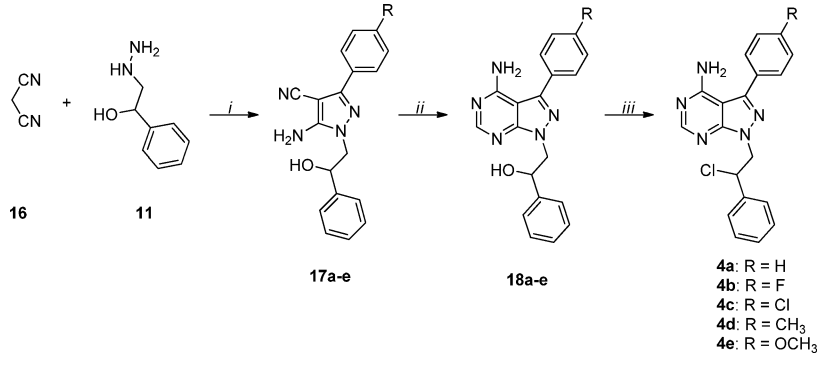

[a]Reagents and conditions: (i) (a) **16**, NaH, anhyd THF, 0/5 °C, 30 min; (b) RC_6H_4COCl, rt, 2−12 h; (c) Me_2SO_4, reflux, 6 h; (d) **11**, reflux, 4 h; (ii) formamide, 190 °C, 3−4 h; (iii) $SOCl_2$, anhyd CH_2Cl_2, rt, 12 h, N_2 atmosphere.

DOI: 10.1021/acs.jmedchem.5b00140
J. Med. Chem. 2015, 58, 4590−4609

Scheme 6. Synthesis of Compounds 5a–e[a]

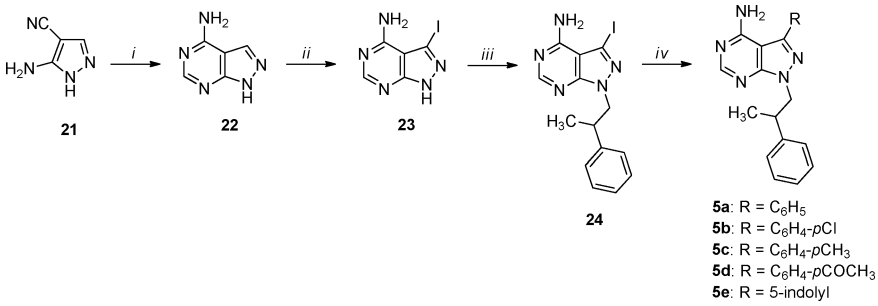

[a]Reagents and conditions: (i) formamide, 200 °C, 1 h; (ii) NIS, anhyd DMF, 80 °C, 14 h, N_2 atmosphere; (iii) 1-bromo-2-phenylpropane, K_2CO_3, anhyd DMF, 130 °C, 18 h; (iv) boronic acids, Cs_2CO_3, $PdCl_2$(dppf), anhyd toluene, 90 °C, 14 h.

Scheme 7. Synthesis of Compounds 6a–b[a]

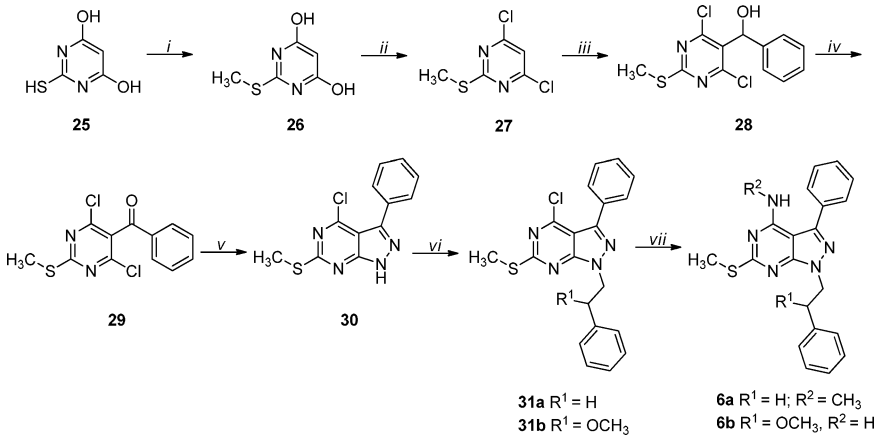

[a]Reagents and conditions: (i) KOH, MeI, H_2O, reflux, 3 h; (ii) $POCl_3$, reflux, 12 h, N_2 atmosphere; (iii) LDA, −78 °C, anhyd THF then PhCHO; (iv) MnO_2, toluene, 1 h; (v) TEA, N_2H_4 H_2O, dioxane, rt, 1 h; (vi) 2-phenylethanol or 2-methoxy-2-phenylethanol, Ph_3P, DIAD, anhyd THF, MW 100 °C, 3 min; (vii) R^2NH_2, EtOH, reflux, 12 h.

Suzuki cross-coupling because the one-pot reaction previously described led to very low yields. 5-Amino-1*H*-pyrazolo-4-carbonitrile **21**,[42] obtained by reaction of (ethoxymethylene)-malononitrile with hydrazine monohydrate, was cyclized by reaction with formamide at 200 °C for 1 h, affording 1*H*-pyrazolo[3,4-*d*]pyrimidin-4-amine **22**.[42] Reaction of **22** with *N*-iodosuccinimide (NIS) in dry DMF at 80 °C for 14 h under nitrogen atmosphere gave 3-iodo-1*H*-pyrazolo[3,4-*d*]pyrimidin-4-amine **23**.[43] This last was in turn treated with K_2CO_3 and 1-bromo-2-phenylpropane at 130 °C for 18 h to afford 3-iodo-1-(2-phenylpropyl)-1*H*-pyrazolo[3,4-*d*]pyrimidin-4-amine **24** in good yield. Finally, compound **24** was reacted with an excess of the suitable boronic acid in the presence of Cs_2CO_3 and $PdCl_2$(dppf) in dry toluene at 90 °C for 14 h to give compounds **5a–e** (Scheme 6).

Compounds **6a** and **6b**, characterized by a phenylethyl and 2-methoxy-2-phenylethyl chain on the N1 position and bearing a *S*-methyl moiety on C6, have been synthesized following the procedure recently reported by us (Scheme 7).[37] Starting from thiobarbituric acid **25**, first the thiol moiety was methylated to afford the intermediate **26** that was chlorinated with $POCl_3$, giving compound **27**. The 4,6-dichloro-2-(methylthio)-pyrimidine **27** was reacted with LDA and benzaldehyde to give the alcohol **28**, subsequently oxidized to the ketone **29**. The latter was cyclized to afford the pyrazole[3,4-*d*]pyrimidine core (**30**) by using hydrazine monohydrate. Mitsunobu reaction with 2-phenylethanol or 2-methoxy-2-phenylethanol was performed in order to introduce the N1 substituent, leading to compounds **31a** and **31b**. These were reacted with *N*-methylamine or ammonia to afford the final compounds **6a** and **6b**, respectively.

Biology. *Selectivity against a Human Kinase Panel.* To assess its specificity against Fyn, compound **4c** was tested against a panel of kinases including other Src family members (Hck, Blk, Fgr, Fyn, Src, Lck, Lyn, and Yes), tyrosine kinases (Abl, EGFR, IGF1R, JAK2, PDGFR, KDR), as well as some serine–threonine kinases. The percentage of enzymatic activity was measured for each kinase by using **4c** at 10 μM (Millipore); results are listed in Table 7. Remarkably, **4c** proved to be more efficient against Src family members than toward the other investigated kinases, confirming such a compound as a useful probe to study Src family function. Furthermore, a high activity against Abl was also detected as expected for the high structural similarity between Abl and the SFKs. Notably, **4c** was not able to significantly inhibit any of the serine–threonine kinases tested (Pim-1, mTOR, JNK, CDK5, Chl1), resulting as not active also toward the serine–threonine kinases DYRK1a and GSK3-β that were reported as implicated in AD.[44,45]

Biological Evaluation in an Alzheimer's Disease Model. In AD Fyn mediates the phosphorylation of Tau on the Tyr18 residue, an early and crucial step in the disease progression, and is therefore considered a promising therapeutic target.[12] For this reason, the most interesting compounds identified during in vitro inhibition assays, **4c** and **4d**, were evaluated for their

DOI: 10.1021/acs.jmedchem.5b00140
J. Med. Chem. 2015, 58, 4590–4609

Table 7. Kinase Profiling of Compound 4c

	residual activity (%)[a]
Fyn (h)	1
Abl (h)	9
Abl (H396P) (h)	5
Abl (M351T) (h)	6
Abl (Q252H) (h)	3
Abl(T315I) (h)	97
Abl(Y253F) (h)	2
Blk (h)	19
CDK5/p25 (h)	86
CDK5/p35 (h)	99
CHK1 (h)	97
cKit (h)	36
cSRC (h)	17
EGFR (h)	47
Fgr (h)	4
GSK3β (h)	66
Hck (h)	7
Hck (h) activated	2
IGF-1R (h)	71
JAK2 (h)	118
JNK3 (h)	53
KDR (h)	31
Lck (h)	2
Lck (h) activated	9
Lyn (h)	15
mTOR (h)	47
PDGFRβ (h)	51
Pim-1 (h)	91
Src(1−530) (h)	2
Src(T341M) (h)	98
Yes (h)	5
Dyrk1a	85

[a]Residual kinase activity after treatment with **4c** at 10 μM, expressed as percent of basal kinase activity.

ability to inhibit the Fyn mediated phosphorylation of residue Tyr18 in Tau protein in an AD model cell line. To this aim, neuroblastoma SH-SY5Y cells were differentiated to mature neurons with the administration of retinoic acid, followed by brain derived neurotrophic factor, neuregulin β1, nerve growth factor, and vitamin D3 treatment. Once differentiated, SH-SY5Y cells were treated[46] with amyloid beta 1−42 ($A\beta_{42}$) oligomer/protofibril in order to induce AD-like neurotoxicity.[47,48] Both compounds significantly affected $A\beta_{42}$ induced Tyr18-Tau phosphorylation with a similar degree and in a dose-dependent manner (Figure 6). Moreover, the inhibitory activity of **4c** and **4d** resulted as being constant over time, being effective up to 6 h after compound administration (Figure 6, compare panels A and B with panels C and D).

Anticancer Activity. The three most active compounds in terms of enzymatic activities, **4b**, **4c**, and **4d**, were then evaluated for their antiproliferative activity on the human CML cell line K562 (Table 3). Several members of the Src kinase family are upregulated and/or hyperactivated in CML, and their activity regulates proliferation and differentiation of cancer cells. In K562 cells, Fyn kinase expression is under the direct control of Bcr-Abl oncogene and its upregulation is fundamental in sustaining K562 proliferation.[23] The tested compounds showed an effective antiproliferative activity that well correlates with the K_i values determined by in vitro inhibition assays. The most effective compounds, **4c** and **4d**, showed promising IC_{50} values in the submicromolar range for cell viability. Moreover, antitumoral effect of **4c** and **4d** was evaluated through cell cycle analysis (Figure 7). K562 cells were treated with increasing concentration of each compound (0.01−1 μM), and the percentage of cells in each phase of cell cycle was evaluated by cytofluorimetric analysis of DNA content. Both compounds determined a significant and dose-dependent accumulation of cells in the G1 phase of cell cycle starting from 0.01 μM. In parallel, we observed a progressive accumulation of hypodiploid cells, indicating the presence of apoptotic cells. Notably, the treatment with 0.1 μM **4d** induced the apoptosis in about 50% of treated K562 cells. Compounds **4c** and **4d** were also tested on early hematopoietic progenitors (CD34+) from Ph+ CML patient who developed resistance to both Imatinib mesylate and Dasatinib. Cells were seeded at 2 ×

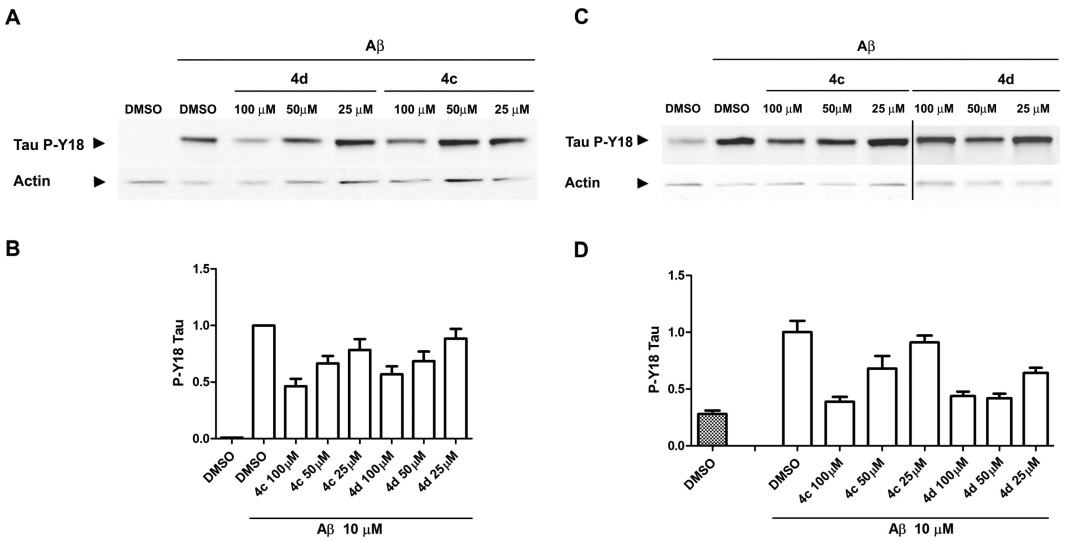

Figure 6. 4c and **4d** inhibit $A\beta_{42}$ mediated phosphorylation of Tyr18-Tau in differentiated SH-SY5Y cells. Western blot analysis of $A\beta_{42}$ mediated phosphorylation of Tyr18-Tau was performed after 1.5 (A) or 6 h (C) from administration of different amount of compounds **4c** and **4d**. (B,D) Data were quantified by chemiluminescence. Experiments were conducted in triplicate, error bars represent ± SEM.

DOI: 10.1021/acs.jmedchem.5b00140
J. Med. Chem. 2015, 58, 4590−4609

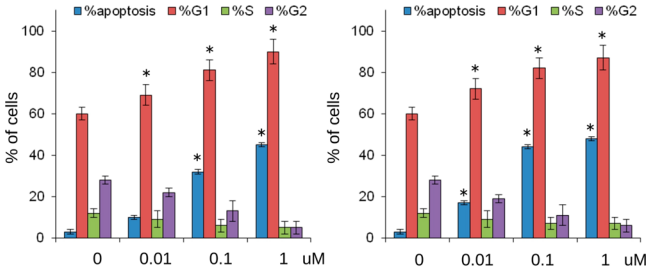

Figure 7. Analysis of the cell cycle distribution of K562 cells after treatment with increasing concentrations of **4c** and **4d**. K562 cells status was investigated by cytofluorimetry analysis of DNA content, and results were expressed as percentage of cells in each phase of cell cycle respect to total viable cells. Apoptosis was evaluated by calculating the number of hypodiploid cells and was expressed as percentage of apoptotic cells respect to total cells (viable and dead cells). Results are the mean of three different experiments. *$p < 0.01$ with respect to the value of the untreated cells.

10^5 cells/mL density and treated with Imatinib 1 μM, and **4c−d** at 2 μM concentration for 48 h. The percentage of apoptotic CD34+ after Imatinib treatment was found equal to control, confirming drug resistance. By contrast, **4c** and **4d** increased apoptotic levels to 35% and 30%, respectively (Figure 8). It is

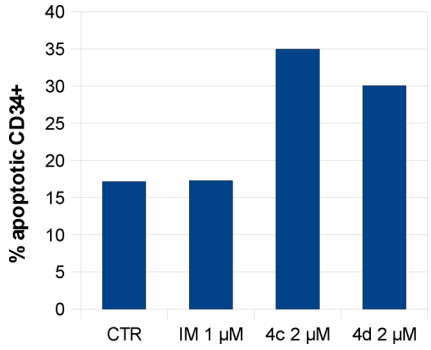

Figure 8. Percentage of apoptotic CD34+ cells from bone marrow sample of CML patient resistant to Imatinib after treatment with Imatinib 1 μM **4c** and **4d** at 2 μM concentration for 48 h.

important to note that these compounds, when tested in human normal fibroblasts, did not show any sign of cell toxicity. In the same way, the viability of differentiated neuron, in the absence of Aβ_{42} treatment, resulted in not being affected by the administration of **4c** and **4d** (data not shown). On the other hand, we also evaluated our compound on two solid human tumor cell lines, MDA-MD-231 (human breast cancer cell line) and U87 (human glioblastoma multiforme cell line), that have previously been described as dependent on SFKs for their proliferation. Cell lines were treated with different dilutions of **4c** and **4d**, and cell viability and proliferation were measured considering real-time impedance generated by cells growing in electric plates. Treated cells showed similar response profiles with significant difference in cell growth starting from 20 h after treatment with respect to control cells and with a more evident inhibition of cell viability from 70 h after treatment (Figure 9). U87 cells resulted particularly responsive to SFKs inhibitors, with **4c** and **4d** treatment that resulted in IC_{50} values of 0.074 and 0.78 μM, respectively. The tested **4c** and **4d** compounds also showed an effective antiproliferative activity on the MDA-MD-231 cell line, with IC_{50}s in the low micromolar range (3.7 and 8.3 μM for compounds **4c** and **4d**, respectively).

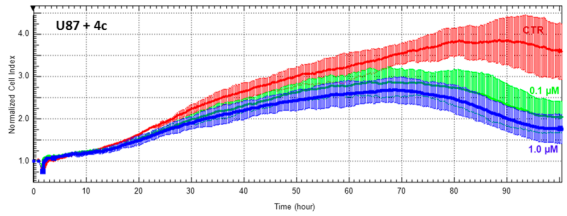

IC_{50} 72h ± SD (μM)	4c	4d
MDA-MB-231	3.7±0.5	8.3±2.1
U87	0.074±0.03	0.78±0.2

Figure 9. Real-time cell viability of MDA-MB-231 and U87 cell lines was evaluated by RTCA iCELLigence system. In the graph, a representative growth profile (with SD) obtained with U87 cells treated with 0.1 (green line) and 1 μM (blue line) **4c** with respect to control cells (red line) are shown. The time scale starts from the treatment (time = 0 h). The IC_{50} was calculated considering the variation of Cell Index within 72 h of incubation.

In Vitro ADME Study. Compounds **4a−e** were profiled in vitro for aqueous solubility, liver microsomal stability, and membrane permeability (Table 8). Their aqueous solubility (−log *S* ranging from 7.26 to 8.25) was very weak and constituted a deleterious parameter in terms of suitable PK profile. However, passive membrane permeability in a PAMPA assay indicated a good cell permeability for compounds **4a−e** (ranging from 9.9 to 17.5 × 10^{-6} cm/s). Similarly, all of these compounds were found to cross the blood−brain barrier (BBB) in a specific PAMPA-BBB assay with good permeability values (ranging from 8.4 to 14.5 × 10^{-6} cm/s). Moreover, stability tests disclosed that all analogues showed good (from 78.9 to 95.6%) metabolic stability in liver microsomes. Metabolite identification by LC-MS analysis after incubation in human microsomes indicated the primary metabolites were actually the products of an oxidative dehalogenation (Table 9) at the chlorine atom in the N1 side chain as previously reported by us for similar compounds.[49]

CONCLUSIONS

Because of its central role in AD pathogenesis and in various human cancers, Fyn kinase could be surely considered an interesting target for therapeutic intervention. In the present work, molecular modeling calculations and organic synthesis were combined together toward the discovery of novel and potent Fyn inhibitors targeting the ATP binding site. A structure-based virtual screening approach was initially applied on commercial libraries and led to the identification of two hit compounds which showed K_i values in the low micromolar range. Remarkably, one of these Fyn inhibitors was characterized by an original chemical scaffold, never discovered before in the field of kinase. The same computational strategy based on the use of docking analysis on an internal library of dual Src/Abl kinase inhibitors allowed as to identify a 3-substituted pyrazolo[3,4-*d*]pyrimidine with a K_i of 0.9 μM. An increase in the in vitro binding affinity of such compound toward Fyn was then rapidly obtained by the synthesis of a small family of analogues. The best identified inhibitors, having nanomolar K_i, were then tested in cell-based assays where they showed interesting cell growth inhibitory activities in an antiproliferative assay carried out on the K562 cell line of CML. Selected compounds were also found to be active against a CML cell line derived from a patient resistant to both Imatinib mesylate and Dasatinib. Interesting antiproliferative activities of SFK inhibitors reported herein were also detected

DOI: 10.1021/acs.jmedchem.5b00140
J. Med. Chem. 2015, 58, 4590−4609

Table 8. In Vitro ADME Profile of Compounds 4a−e[a]

compd	PAMPA[b] $P_{app} \times 10^{-6}$ (cm/s)	PAMPA-BBB[b] $P_{app} \times 10^{-6}$(cm/s)	water solubility (log S)[c]	metabolic stability[d] (%)	major metabolites[e,f] (%)
4a	12.8	9.5	−7.26	78.9	M1 = M-36 + 16 (18.0)
					M2 = M-35 + 17 (3.0)
4b	16.5	12.9	−7.75	95.7	M1 = M-36 + 16 (2.8)
					M2 = M-35 + 17 (1.4)
4c	9.9	8.4	−7.60	85.2	M1 = M-36 + 16 (14.7)
					M2 = M-35 + 17 (<0.10)
4d	10.9	11.5	−7.30	90.0	M1 = M-36 + 16 (2.4)
					M2 = M-35 + 17 (5.0)
					M3 = M+16 (2.6)
4e	17.5	14.5	−8.25	95.6	M1 = M-36 + 16 (2.5)
					M2 = M-35 + 17 (0.9)
					M4 = −14 (0.8)
caffeine		1.12			

[a]Caffeine was used as reference compound. [b]PAMPA see Experimental Section for details. [c]log S = log mol L^{-1}. [d]Expressed as percentage of unmodified parent drug. [e]M = mass of the parent drug; M1−4 = experimental mass of the identified metabolites. [f]The structure of each metabolite is reported in Table 9.

Table 9. Structures of Identified Metabolites for Compounds 4a−e

Name	Structure	M1	M2	M3	M4
4a	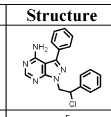			-	-
4b	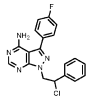	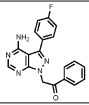	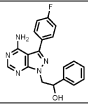	-	-
4c	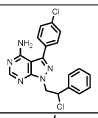	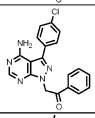	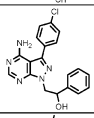	-	-
4d	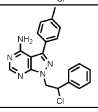	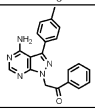	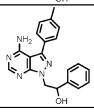	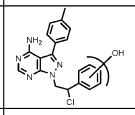	-
4e	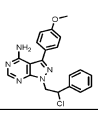	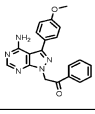	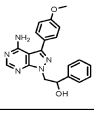	-	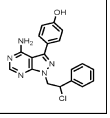

on solid tumors and in particular against glioblastoma, on which the best compound showed an IC_{50} of 70 nM. On the other hand, the studied compounds showed appreciable activities in an AD model cell line as a consequence of the inhibition of the Fyn-mediated phosphorylation of the Tau protein. Taken together, the ability of these compounds to potently inhibit the SFKs also in cell-based assays, in addition to their promising toxicity profile, suggest that 3-susbtituted pyrazolo[3,4-*d*]-pyrimidines could already be considered as promising early agents to be further investigate for the treatment of cancer and AD. Furthermore, the high penetration through the BBB is a favorable feature for the effective use of such compounds for the treatment of AD or glioblastoma.

EXPERIMENTAL SECTION

Computational Details. *Protein Preparation.* The Fyn three-dimensional coordinates was selected from the Protein Data Bank (PDB entry code 2DQ7)[50] and was prepared by means of Protein Preparation Wizard workflow implemented in Maestro suite.[51] In particular, the inhibitor and the water molecules were deleted, hydrogen atoms were added, and bond orders and charges were assigned; the orientation of hydroxyl groups on Ser, Thr, and Tyr, the side chains of Asn and Gln residues, and the protonation state of His residues were optimized. Steric clashes were relieved by performing a small number of minimization steps, not intended to minimize the system completely. In our study, the minimization (OPLS force field) was stopped when the RMSD of the non-hydrogen atoms reached 0.30 Å.

Ligand Preparation. A series of about 300 pyrazolo[3,4-*d*]-pyrimidines was collected from previous work and were built with the Schrodinger Maestro 9.2 graphical interface.[51] Compounds were then processed with the Schrodinger LigPrep[52] tool to generate separate files for all possible enantiomers and protonation states at physiological pH. OPLS_2005 was used as force field. The same procedure was used on the reference ligands staurosporine, PP1 and PP2.

Concerning the three-dimensional structure of the commercially available compounds, we retrieved them from ZINC[53] database by selecting Asinex as vendor. Compounds analyzed were 703200, belonging to both Gold and Synergy collections.

Docking Simulation. Docking studies were performed within the ATP binding site of Fyn kinase using the software package Gold 4.1.[54] The binding pocket was inserted into a grid box centered on the bound ligand Staurosporine and enclosing residues lying within about 8 Å from the ligand itself. Chemscore was chosen as the fitness function for docking calculation. The genetic algorithm parameter settings were employed using the search efficiency set at 100%, and different number of runs were carried out for each ligand depending on the stage of VS (for the first step of the VS of the ASINEX database the value was set to 10, while for the second step and for the VS of pyrazolo[3,4-*d*]pyrimidine library the value was set to 100). Finally, results differing less than 1 Å in ligand−all atom RMSD were clustered together. For each inhibitor, the first ranked solution as well as the lowest energy conformation of the most populated cluster were selected for further analysis. The known ligands staurosporine, PP1 and PP2, were also docked to validate the docking protocol. The binding mode predicted for such ligands was in perfect agreement with that experimentally determined for the same molecules within the ATP binding site of Src-family kinases.[50,55,56]

Molecular Dynamic Simulation (MD). Molecular dynamics simulations were performed starting from the best docking poses of compounds **4a−d** and PP2 within the ATP binding site of Fyn kinase. The parametrization of ligands was performed by means of the *antechamber* module of Amber 11.[57] The Generalized Amber Force Field (GAFF)[58] was used to assign the atom type for each molecule, while the charges were assigned using AM1-BCC method.[59] The parametrization of the protein was performed by means of *leap* module of Amber 11 using the ff99SB force field. The parameters set for phosphotyrosine of the activation loop were that published by Homeyer and collegues.[60] Hydrogens were added at each complex,

DOI: 10.1021/acs.jmedchem.5b00140
J. Med. Chem. 2015, 58, 4590−4609

which, subsequently, was solvated in a TIP3P octaedric box system of explicit water molecules with a 10 Å buffer. An appropriate number of counterions were added to neutralize the system. The SHAKE algorithm was used to treat hydrogen-containing bonds.[61] Before MD simulations, two steps of energy minimization were performed to remove bad contacts. In the first stage, the protein was kept fixed with a constraint of 500 kcal/mol, and only the water molecules were minimized. In the second stage, the entire system was minimized applying a constraint of 10 kcal/mol on the α-carbon. The two minimization stages consisted of 15000 steps in which the first 1000 were steepest descent and the last were conjugate gradient. MD trajectories were run using the minimized structures as a starting point. Constant volume simulations were performed for 500 ps, during which the temperature was raised from 0 to 300 K using the Langevin dynamics method with a collision frequency of γ = 1.0 ps -1.[62,63]

Then 1500 ps of constant-pressure MD simulations were performed at 300 K in three steps of 500 ps each. During these steps, a decreasing harmonic force constraint of 10, 5, and 1 kcal/mol·Å was applied, respectively. Finally, a 10 ns MD simulations without restraints were run at constant temperature of 300 K and a constant pressure of 1 atm. During the simulations, the Particle Mesh Ewald method was employed to calculate the long-range electrostatic interactions. A 10 Å cutoff value was used for the nonbonded interactions, and a time step of 2 fs was used for the simulations.

The module Ptraj implemented in AMBER 11 was used to analyze trajectories. In particular, RMSD and RMSFs were calculated for the α-carbons of each residue on the production stage. In particular, snapshots have been extracted for the last 6 ns of the production phase of the simulation; one snapshot has been extracted every 10 frames for a total of 150 structures. During the simulation, the hydrogen bonds between ligands and kinase domain were detected when the acceptor−donor atom distance was lower than 3 Å and the occupancy was more than 10% in the investigated time period. The same snapshots were evaluated to evaluate the binding free energy between the preferred poses of ligands and the protein by means of MM/GBSA and MM/PBSA approaches. The entropy term was considered negligible, and it was thus not calculated in this work being computationally expensive.

Chemistry. Starting materials were purchased from Aldrich-Italia (Milan, Italy). Melting points were determined with a Büchi 530 apparatus and are uncorrected. IR spectra were measured in KBr with a PerkinElmer 398 spectrophotometer. ^{1}H NMR spectra were recorded in a $CDCl_3$ solution (unless otherwise specified) on a Varian Gemini 200 (200 MHz) instrument or using a Bruker Avance DPX400 (Bruker Biospin, Germany). Chemical shifts are reported as δ (ppm) relative to TMS as the internal standard, J in Hz. ^{1}H patterns are described using the following abbreviations: s = singlet, d = doublet, t = triplet, q = quartet, m = multiplet, and br s = broad singlet. TLC was carried out using Merck TLC plates silica gel 60 F254. Chromatographic purifications were performed on columns packed with Merk 60 silica gel, 23−400 mesh, for flash technique. Analyses for C, H, N, and S were within ±0.3% of the theoretical value. Mass spectra (MS) data were obtained using an Agilent 1100 LC/MSD VL system (G1946C) with a 0.4 mL/min flow rate using a binary solvent system of 95:5 methanol/water. UV detection was monitored at 254 nm. MS were acquired in positive and negative modes, scanning over the mass range 50−1500. The following ion source parameters were used: drying gas flow, 9 mL/min; nebulizer pressure, 40 psig; drying gas temperature, 350 °C. All target compounds possessed a purity of ≥95% as verified by elemental analyses by comparison with the theoretical values.

Compounds **3a−c**,[29] **3d**,[64] **3e**,[30] **3f−i**, **10**,[31] **3p**,[32] **3q**, **3s**, **7**, **8a**, **9a**,[65] **3r**,[24] **8c** and **9c**,[29] **12**, and **13**[40] have been already reported by us.

General Procedure for the Synthesis of Compounds 3j and 3k. The suitable amine (4 mmol) was added to a solution of 4-chloro derivative **9b** (381 mg, 1 mmol) in anhydrous toluene (5 mL), and the mixture was stirred at room temperature for 48 h. The organic phase was washed with water (2 × 10 mL), dried ($MgSO_4$), filtered, and concentrated under reduced pressure. The crude oil was purified by column chromatography (Florisil, 100−200 mesh) using diethyl ether as the eluent. The compounds crystallized by adding a 1:1 mixture of Et_2O/petroleum ether (PE) (bp 40−60 °C).

*N-Benzyl-6-(sec-Butylthio)-1-(2-chloro-2-phenylethyl)-1H-pyrazolo[3,4-d]pyrimidin-4-amine (**3j**).* White solid (271 mg, 60%); mp 112−113 °C. ^{1}H NMR: δ 1.05 (t, J = 7.2 Hz, 3H, $CH_2\underline{CH_3}$), 1.42−1.45 (m, 3H, $CH\underline{CH_3}$), 1.68−1.74 and 1.80−1.85 (2m, 2H, $\underline{CH_2}CH_3$), 3.81−3.84 (m, 1H, SCH), 4.68−4.88 (m, 4H, CH_2N + CH_2Ar), 5.49−5.53 (m, 1H, CHCl), 7.24−7.41 (m, 10H Ar), 7.69 (s, 1H, H-3). IR (cm^{-1}): 3250 (NH). MS: m/z [M + 1]$^+$ 453. Anal. ($C_{24}H_{26}N_5ClS$) C, H, N, S.

*6-(sec-Butylthio)-1-(2-chloro-2-phenylethyl)-N-(2-phenylethyl)-1H-pyrazolo[3,4-d]pyrimidin-4-amine (**3k**).* White solid (368 mg, 79%); mp 97−98 °C. ^{1}H NMR: δ 1.03 (t, J = 7.0 Hz, 3H, $CH_2\underline{CH_3}$), 1.34−1.50 (m, 3H, $CH\underline{CH_3}$), 1.59−1.83 (m, 2H, $\underline{CH_2}CH_3$), 2.91 (t, J = 6.2 Hz, 2H, CH_2Ar), 3.70−3.88 (m, 3H, SCH + $\underline{CH_2}NH$), 4.60−4.90 (m, 2H, CH_2N), 5.30 (br s, 1H, NH disappears with D_2O), 5.41−5.54 (m, 1H, CHCl), 7.04−7.41 (m, 10H Ar), 7.63 (s, 1H, H-3). IR (cm^{-1}): 3255 (NH). MS: m/z [M + 1]$^+$ 467. Anal. ($C_{25}H_{28}N_5ClS$) C, H, N, S.

6-(*sec*-Butylthio)-*N*-(3-chlorophenyl)-1-(2-chloro-2-phenylethyl)-1*H*-pyrazolo[3,4-*d*]pyrimidin-4-amine (3l). *m*-Chloroaniline (255 mg, 2 mmol) was added to a solution of the 4-chloro derivative **9b** (381 mg, 1 mmol) in absolute ethanol (5 mL), and the mixture was refluxed for 5 h. After cooling to room temperature, the obtained solid was filtered, washed with water, and recrystallized from absolute ethanol. White solid (236 mg, 50%); mp 213−214 °C. ^{1}H NMR: δ 1.02 (t, J = 7.0 Hz, 3H, $CH_2\underline{CH_3}$), 1.40−1.44 (m, 3H, $CH\underline{CH_3}$), 1.65−1.80 (m, 2H, $\underline{CH_2}CH_3$), 3.80−3.85 (m, 1H, SCH), 4.75−4.80 and 4.87−4.93 (2m, 2H, CH_2N), 5.63−5.67 (m, 1H, CHCl), 7.14−7.66 (m, 9H Ar), 8.30 (s, 1H, H-3), 10.34 (br s, 1H, NH disappears with D_2O). IR (cm^{-1}): 2933 (NH). MS: m/z [M + 1]$^+$ 473. Anal. ($C_{23}H_{23}N_5Cl_2S$) C, H, N, S.

***N*-[2-(3-Chlorophenyl)ethyl]-6-(methylthio)-1-[2-phenylvinyl]-1*H*-pyrazolo[3,4-*d*]pyrimidin-4-amine (3m).** A solution of 4N NaOH (2 mL) was added to a suspension of *N*-[2-(3-chlorophenyl)-ethyl]-1-(2-chloro-2-phenylethyl)-6-(methylthio)-1*H*-pyrazolo[3,4-*d*]-pyrimidin-4-amine **3r** (458 mg, 1 mmol) in 95% ethanol (12 mL), and the mixture was refluxed for 5 h. After cooling, the solid was filtered, washed with water, and recrystallized from absolute ethanol. White solid (273 mg, 65%); mp 104−106 °C. ^{1}H NMR: δ 2.64 (s, 3H, SCH_3), 2.98 (t, J = 5.0 Hz, 2H, CH_2Ar), 3.87 (q, J = 5.0 Hz, 2H, $\underline{CH_2}NH$), 5.52 (br s, 1H, NH disappears with D_2O), 7.09−7.50 (m, 10H, 9Ar + CH═), 7.92 (s, 1H, H-3), 7.96 (d, J_{trans} = 16.0 Hz, 1H, CH═). IR (cm^{-1}): 3269 (NH), 1663 (C═C). MS: m/z [M + 1]$^+$ 423. Anal. ($C_{22}H_{20}N_5ClS$), C, H, N, S.

2-(4-Benzylamino-1-styryl-1*H*-pyrazolo[3,4-*d*]pyrimidin-6-ylamino)-ethanol (3n). Ethanolamine (180 μL, 3 mmol) was added to a suspension of **10** (405 mg, 1 mmol) in butan-1-ol (16 mL) and DMSO (4 mL), and the mixture was heated at 90 °C for 12 h. After cooling to room temperature, butan-1-ol was removed under reduced pressure, then water (20 mL) was added and the solution was extracted with ethyl acetate (2 × 20 mL); the organic phase was washed with water (20 mL), dried ($MgSO_4$), and evaporated under reduced pressure. The obtained solid was filtered and recrystallized from absolute ethanol. White solid (255 mg, 66%); mp 148−149 °C. ^{1}H NMR: δ 3.68 (q, J = 4.8 Hz, 2H, CH_2), 3.88 (q, J = 4.8 Hz, 2H, CH_2), 4.77 (d, J = 4.6 Hz, 2H, CH_2Ar), 5.63 (br s, 1H, NH, disappears with D_2O), 7.22−7.54 (m, 11H, 10Ar + CH═), 7.78 (s, 1H, H-3), 7.82 (d, J_{trans} = 17.2 Hz, 1H, CH═). IR (cm^{-1}): 3281−3025 (OH + NH), 1657 (C═C). MS: m/z [M + 1]$^+$ 387. Anal. ($C_{22}H_{22}N_6O$) C, H, N.

***N*,6-Dibenzyl-1-(2-chloro-2-phenylethyl)-1*H*-pyrazolo[3,4-*d*]pyrimidin-4-amine (3o).** Benzylamine (440 μL, 4 mmol) was added to a solution of 4-chloro derivative **15** (383 mg, 1 mmol) in anhydrous toluene (5 mL), and the mixture was stirred at room temperature for 48 h. The organic phase was washed with water (2 × 10 mL), dried ($MgSO_4$), filtered, and concentrated under reduced pressure. The crude oil was crystallized by adding a 1:1 mixture of Et_2O/PE (bp 40−60 °C) to give **3o**. White solid (250 mg, 55%); mp 125 °C. ^{1}H NMR: δ 4.00 (s, 2H, CH_2Ar), 4.53−4.96 (m, 4H, CH_2N +

DOI: 10.1021/acs.jmedchem.5b00140
J. Med. Chem. 2015, 58, 4590−4609

NHCH$_2$Ar), 5.40−5.54 (m, 1H, CHCl), 7.00−7.73 (m, 15H Ar), 8.04 (s, 1H, H-3). IR (cm^{-1}): 3255 (NH) MS: *m/z* [M + 1]$^+$ 455. Anal. ($C_{27}H_{24}N_5Cl$) C, H, N.

General Procedure for the Synthesis of 4a−e. $SOCl_2$ (80 μL, 1.1 mmol) was added dropwise to a solution of the suitable intermediate **18a−e** (0.5 mmol) in dry CH_2Cl_2 (5 mL), and the reaction was stirred at room temperature for 12 h under nitrogen atmosphere. Water (5 mL) and 1N NaOH (1 mL) were added with caution, and the aqueous phase was extracted with CH_2Cl_2 (2 × 5 mL). Then the organic phase was washed with water (5 mL) and brine (5 mL), dried (Na_2SO_4), and concentrated under reduced pressure. Compounds **4b−e** were obtained as white solids, adding a 1:1 mixture of Et_2O/PE (bp 40−60 °C). Compound **4a**, that resulted in a yellow oil, was precipitated as hydrochloride salt by adding a saturated solution of HCl in dry Et_2O.

*1-(2-Chloro-2-phenylethyl)-3-phenyl-1H-pyrazolo[3,4-d]pyrimidin-4-amine hydrocloride (**4a**).* White solid (135 mg, 70%); mp 129−132 °C. ^{1}H NMR: δ 4.76−4.81 and 5.00−5.06 (2m, 2H, CH$_2$N), 5.50−5.54 (m, 1H, CHCl), 7.23−7.73 (m, 10H Ar), 9.49 (s, 1H, H-6). MS: *m/z* 387 [M + 1]$^+$. Anal. ($C_{19}H_{17}N_5Cl_2$) C, H, N.

*1-(2-Chloro-2-phenylethyl)-3-(4-fluorophenyl)-1H-pyrazolo[3,4-d]pyrimidin-4-amine (**4b**).* White solid (125 mg, 68%); mp 203−206 °C. ^{1}H NMR: δ 4.77−4.82 and 4.95−5.00 (2m, 2H, CH$_2$N), 5.68−5.70 (m, 1H, CHCl), 7.38−7.42 and 7.51−7.64 (m, 9H Ar), 8.22 (s, 1H, H-6). IR (cm^{-1}): 3477, 3314 (NH$_2$). MS: *m/z* 369 [M + 1]$^+$. Anal. ($C_{19}H_{15}N_5ClF$) C, H, N.

*3-(4-Chlorophenyl)-1-(2-chloro-2-phenylethyl)-1H-pyrazolo[3,4-d]pyrimidin-4-amine (**4c**).* White solid (65 mg, 34%); mp 150−151 °C. ^{1}H NMR: δ 4.76−4.80 and 4.97−5.02 (2m, 2H, CH$_2$N), 5.67−5.68 (m, 1H, CHCl), 7.34−7.36 and 7.51−7.61 (m, 9H Ar), 8.24 (s, 1H, H-6). IR (cm^{-1}): 3470, 3301 (NH$_2$). MS: *m/z* 385 [M + 1]$^+$. Anal. ($C_{19}H_{15}N_5Cl_2$) C, H, N.

*1-(2-Chloro-2-phenylethyl)-3-(4-methylphenyl)-1H-pyrazolo[3,4-d]pyrimidin-4-amine (**4d**).* White solid (90 mg, 49%); mp 159−160 °C. ^{1}H NMR: δ 2.36 (s, 3H, CH$_3$), 4.75−4.80 and 4.95−5.01 (2m, 2H, CH$_2$N), 5.66−5.70 (m, 1H, CHCl), 7.24−7.39 and 7.50−7.63 (m, 9H Ar), 8.23 (s, 1H, H-6). IR (cm^{-1}): 3468, 3306 (NH$_2$). MS: *m/z* 365 [M + 1]$^+$. Anal. ($C_{20}H_{18}N_5Cl$) C, H, N.

*1-(2-Chloro-2-phenylethyl)-3-(4-methyoxyphenyl)-1H-pyrazolo-[3,4-d]pyrimidin-4-amine (**4e**).* White solid (146 mg, 77%); mp 152−153 °C. ^{1}H NMR: δ 3.89 (s, 3H, OCH$_3$), 4.75−4.80 and 5.01−5.07 (2m, 2H, CH$_2$N), 5.58−5.62 (m, 1H, CHCl), 7.01−7.10 and 7.26−7.68 (m, 9H Ar), 8.36 (s, 1H, H-6). IR (cm^{-1}): 3470, 3305 (NH$_2$). MS: *m/z* 381 [M + 1]$^+$. Anal. ($C_{20}H_{18}N_5ClO$) C, H, N.

General Procedure for the Synthesis of 5a−e. The suitable boronic acid (1.08 mmol) was added to a suspension of 3-iodo-1-(2-phenylpropyl)-1*H*-pyrazolo[3,4-*d*]pyrimidin-4-amine **24** (100 mg, 0.27 mmol) in dry toluene (5 mL), and the mixture was stirred at room temperature under nitrogen atmosphere for 10 min. Then Cs_2CO_3 (350 mg, 1.07 mmol) and $PdCl_2$(dppf) (20 mg, 10% mol) were added. The reaction was stirred at 90 °C for 14 h. After cooling to room temperature, water (70 mL) was added and the aqueous suspension was extracted with AcOEt (2 × 40 mL). The organic phase was washed with water (40 mL) and brine (40 mL), dried (Na_2SO_4), and concentrated under reduced pressure to obtain a crude, which was purified by column chromatography (silica gel 0.060−0.200 mm, 40 Å) using a mixture of CH_2Cl_2/MeOH (95:5) as the eluent to afford compounds **5a−e**.

*3-Phenyl-1-(2-phenylpropyl)-1H-pyrazolo[3,4-d]pyrimidin-4-amine (**5a**).* White solid (24 mg, 27%); mp 105−109 °C. ^{1}H NMR: δ 1.28 (d, *J* = 6.8 Hz, 3H, CH$_3$), 3.60−3.65 (m, 1H, CH), 4.56−4.62 (m, 2H, CH$_2$N), 5.58 (br s, 2H, NH$_2$ disappears with D$_2$O), 7.17−7.27 and 7.46−7.67 (2m, 10H Ar), 8.40 (s, 1H, H-6). IR (cm^{-1}): 3476, 3298 (NH$_2$). MS: *m/z* 330 [M + 1]$^+$. Anal. ($C_{20}H_{19}N_5$) C, H, N.

*3-(4-Chlorophenyl)-1-(2-phenylpropyl)-1H-pyrazolo[3,4-d]-pyrimidin-4-amine (**5b**).* Yellow solid (42 mg, 43%); mp 153−154 °C. ^{1}H NMR: δ 1.27 (d, *J* = 6.8 Hz, 3H, CH$_3$), 3.46−3.62 (m, 1H, CH), 4.50−4.60 (m, 2H, CH$_2$), 5.74 (br s, 2H, NH$_2$ disappears with D$_2$O), 7.18−7.25, 7.41−7.49 and 7.51−7.61 (3m, 9H Ar), 8.33 (s, 1H, H-6). IR (cm^{-1}): 3470, 3421 (NH$_2$). MS: *m/z* 365 [M + H]$^+$. Anal. ($C_{20}H_{18}N_5Cl$) C, H, N.

*3-(4-Methylphenyl)-1-(2-phenylpropyl)-1H-pyrazolo[3,4-d]-pyrimidin-4-amine (**5c**).* Light-brown solid (30 mg, 32%); mp 152−155 °C. ^{1}H NMR: δ 1.27 (d, *J* = 4.4 Hz, 3H, CHCH$_3$), 2.43 (s, 3H, CH$_3$Ar), 3.47−3.66 (m, 1H, CH), 4.55−4.57 (m, 2H, CH$_2$), 5.31 (br s, 2H, NH$_2$ disappears with D$_2$O), 7.18−7.20, 7.32−7.44 and 7.53−7.55 (3m, 9H Ar), 8.34 (s, 1H, H-6). IR (cm^{-1}): 3480, 3325 (NH$_2$). MS: *m/z* 344 [M + H]$^+$. Anal. ($C_{21}H_{21}N_5$) C, H, N.

*1-{4-[4-Amino-1-(2-phenylpropyl)-1H-pyrazolo[3,4-d]pyrimidin-3-yl]phenyl}ethanone (**5d**).* Yellow solid (50 mg, 50%); mp 232−235 °C. ^{1}H NMR: δ 1.29 (d, *J* = 6.8 Hz, 3H, CHCH$_3$), 2.67 (s, 3H, CH$_3$CO), 3.58−3.65 (m, 1H, CH), 4.58−4.60 (m, 2H, CH$_2$), 5.47 (br s, 2H, NH$_2$ disappears with D$_2$O), 7.19−7−27, 7.77−7.79 and 8.11−8.13 (3m, 9H Ar), 8.37 (s, 1H, H-6). IR (cm^{-1}): 3478, 3315 (NH$_2$). MS: *m/z* 372 [M + H]$^+$. Anal. ($C_{22}H_{21}N_5O$) C, H, N.

*3-(1H-Indol-5-yl)-1-(2-phenylpropyl)-1H-pyrazolo[3,4-d]-pyrimidin-4-amine (**5e**).* Light-brown solid (30 mg, 30%); mp 240−241 °C. ^{1}H NMR: δ 1.26 (d, *J* = 7.2 Hz, 3H, CH$_3$), 3.49−3.74 (m, 1H, CH), 4.56−4.59 (m, 2H, CH$_2$), 5.46 (br s, 2H, NH$_2$ disappears with D$_2$O), 6.65 (m, 1H, indole H-3), 7.19−7.26, 7.27−7.32 and 7.49−7.56 (3m, 9H, 8H Ar and 1H, H-2 indole), 7.92 (s, 1H, NH), 8.35 (s, 1H, H-6). IR (cm^{-1}): 3465, 3309 (NH$_2$). MS: *m/z* 369 [M + H]$^+$. Anal. ($C_{22}H_{20}N_6$) C, H, N.

***N*-Methyl-6-(methylthio)-1-phenethyl-3-phenyl-1*H*-pyrazolo[3,4-*d*]pyrimidin-4-amine (6a).** *N*-Methylamine 40% in H_2O (55.6 μL, 0.65 mmol) was added to a solution of **31a** (50.0 mg, 0.13 mmol) in EtOH (10 mL). The reaction solution was stirred under reflux until the starting material disappeared from TLC. The solvent was removed under reduced pressure to obtain a yellow oily residue that was dissolved in EtOAc. The organic phase was extracted twice with 0.5 N HCl. The organic layer was dried (Na_2SO_4) and filtered then the solvent evaporated under reduced pressure to obtain the product as a white solid. White solid (38.9 mg, 81%); mp 103−104 °C. ^{1}H NMR: δ 2.59 (s, 3H, SCH$_3$), 3.06 (s, 3H, NHCH$_3$), 3.23−3.27 (t, *J* = 7.6 Hz, 2H, CH$_2$Ar), 4.60−4.63 (t, *J* = 7.6 Hz, 2H, CH$_2$), 5.34 (br s, 1H, NH, disappears with D$_2$O), 7.29−7.20 (m, 5H Ar), 7.55−7.45 (m, 3H Ar), 7.61−7.63 (d, *J* = 7.2 Hz, 2H Ar). MS: *m/z* [M + 1]$^+$ 376. Anal. ($C_{21}H_{21}N_5S$) C, H, N, S.

1-(2-Methoxy-2-phenylethyl)-6-(methylthio)-3-phenyl-1*H*-pyrazolo[3,4-*d*]pyrimidin-4-amine (6b). In a sealed tube equipped with a rubber septum, to a suspension of **31b** (44.7 mg, 0.11 mmol) in EtOH (1 mL) at −78 °C was added 7 N NH_3 in MeOH (1 mL). The tube was sealed, and the reaction was heated to reflux under nitrogen atmosphere. The solvent was removed under reduced pressure to obtain a solid residue that was purified by flash chromatography using PE/EtOAc (85:15) as the eluent. White solid (39.6 mg, 92%); mp 99−100 °C. ^{1}H NMR: δ 2.56 (s, 3H, SCH$_3$), 3.22 (s, 3H, OCH$_3$), 4.34−4.48 and 4.68−4.74 (m, 2H, CH$_2$), 4.89−4.92 (m, 1H, CH), 5.71 (br s, 2H, NH$_2$, disappear with D$_2$O), 7.27−7.34 (m, 5H Ar), 7.43−7.53 (m, 3H Ar), 7.66−7.67 (d, *J* = 6.8 Hz, 2H Ar). MS: *m/z* [M + 1]$^+$ 392, [M + 23]$^+$ 414. Anal. ($C_{21}H_{21}N_5OS$) C, H, N, S.

6-(*sec*-Butylthio)-1-(2-hydroxy-2-phenylethyl)-1,5-dihydro-4*H*-pyrazolo[3,4-*d*]pyrimidin-4-one (8b). A mixture of 1-(2-hydroxy-2-phenylethyl)-6-thioxo-1,5,6,7-tetrahydro-4*H*-pyrazolo[3,4-*d*]pyrimidin-4-one **7** (2.88 g, 10 mmol), 2-bromobutane (1.11 mL, 10.14 mmol), and anhydrous K_2CO_3 (1.38 g, 10 mmol) in anhydrous DMF (10 mL) was stirred at room temperature for 24 h. The mixture was poured into cold water; the obtained white solid was filtered, washed with water, and recrystallized with ethyl acetate. White solid (1.58 g, 46%); mp 171−172 °C. ^{1}H NMR: δ 1.00 (t, *J* = 7.2 Hz, 3H, CH$_2$CH$_3$), 1.38−1.45 (m, 3H, CHCH$_3$), 1.62−1.78 (m, 2H, CH$_2$CH$_3$), 3.68−3.79 (m, 1H, SCH), 4.25−4.40 (m, 2H, CH$_2$N), 5.10−5.19 (m, 1H, CHOH), 7.18−7.41 (m, 5H Ar), 7.90 (s, 1H, H-3), 12.00 (br s, 1H, NH disappears with D$_2$O). IR (cm^{-1}): 3300−3030 (NH + OH), 1704 (CO). MS: *m/z* [M + 1]$^+$ 345. Anal. ($C_{17}H_{20}N_4O_2S$) C, H, N, S.

6-(*sec*-Butylthio)-4-chloro-1-(2-chloro-2-phenylethyl)-1*H*-pyrazolo[3,4-*d*]pyrimidine (9b). The Vilsmeier complex, previously prepared from $POCl_3$ (9.32 mL, 100 mmol) and anhydrous DMF (7.7

DOI: 10.1021/acs.jmedchem.5b00140
J. Med. Chem. 2015, 58, 4590−4609

mL, 100 mmol), was added to a suspension of 6-(*sec*-butylthio)-1-(2-hydroxy-2-phenylethyl)-1,5-dihydro-4*H*-pyrazolo[3,4-*d*]pyrimidin-4-one **8b** (3.44 g, 10 mmol) in $CHCl_3$ (50 mL). The mixture was refluxed for 8 h. The solution was washed with water (2 × 20 mL), dried ($MgSO_4$), filtered, and concentrated under reduced pressure. The crude oil was purified by column chromatography (Florisil, 100–200 mesh) using diethyl ether as the eluent, to afford the pure product. Yellow oil (1.91 g, 50%). ^{1}H NMR: δ 1.03 (t, J = 7.2 Hz, 3H, $CH_2\underline{CH_3}$), 1.33–1.51 (m, 3H, $CH\underline{CH_3}$), 1.62–1.86 (m, 2H, $\underline{CH_2}CH_3$), 3.67–3.91 (m, 1H, SCH), 4.63–5.00 (m, 2H, CH_2N), 5.36–5.53 (m, 1H, CHCl), 7.11–7.43 (m, 5H Ar), 7.94 (s, 1H, H-3). MS: m/z $[M + 1]^+$ 382. Anal. ($C_{17}H_{18}N_4Cl_2S$) C, H, N, S.

Alternative Procedure for the Synthesis of 5-Amino-1-(2-hydroxy-2-phenylethyl)-1*H*-pyrazole-4-carbonitrile (12). (Ethoxymethylene)malononitrile (2.41 g, 20 mmol) was added to a solution of 2-hydrazino-1-phenylethanol **11** (3 g, 20 mmol) in absolute ethanol (40 mL), and the reaction mixture was irradiated in the microwave oven in open vessel for 5 min at 60 °C, 100 W. After cooling to room temperature, the solvent was concentrated to 50% of the initial volume and cooled to room temperature to give 5-amino-1-(2-hydroxy-2-phenylethyl)-1*H*-pyrazole-4-carbonitrile **12** as a crude. This compound was purified by recrystallization from absolute ethanol. Light-yellow solid (2.97 g, 65%; mp 179–180 °C) (Lit. 63%; mp 180–181 °C).[40]

6-Benzyl-1-(2-hydroxy-2-phenylethyl)-1,5-dihydro-4*H*-pyrazolo[3,4-*d*]pyrimidin-4-one (14). A solution of sodium ethoxide, prepared from sodium (138 mg, 6 mmol) and absolute ethanol (5 mL), and methyl phenylacetate (900 mg, 6 mmol) were added to a solution of 5-amino-1-(2-hydroxy-2-phenylethyl)-1*H*-pyrazole-4-carboxamide **13** (246 mg, 1 mmol) in absolute ethanol (5 mL). The mixture was refluxed for 6 h; after cooling to room temperature, ice water (30 mL) was added and the solution was acidified with 3% acetic acid. The precipitated solid was filtered, washed with water, and recrystallized from absolute ethanol to afford compound **14**. White solid (200 mg, 58%); mp 205–207 °C. ^{1}H NMR: δ 3.98 (s, 2H, CH_2Ar), 4.06 (br s, 1H, OH disappears with D_2O), 4.44–4.51 and 4.55–4.61 (2m, 2H, CH_2N), 5.13–5.18 (m, 1H, $\underline{CH}$OH), 7.16–7.35 (m, 10H Ar), 8.00 (s, 1H, H-3), 10.94 (br s, 1H, NH disappears with D_2O). IR (cm^{-1}): 3440–2893 (OH + NH), 1694 (CO). MS: m/z $[M + 1]^+$ 347. Anal. ($C_{20}H_{18}N_4O_2$) C, H, N.

6-Benzyl-4-chloro-1-(2-chloro-2-phenylethyl)-1*H*-pyrazolo-[3,4-*d*]pyrimidine (15). The Vilsmeier complex, previously prepared from $POCl_3$ (2.80 mL, 30 mmol) and anhydrous DMF (2.3 mL, 30 mmol), was added to a suspension of 6-benzyl-1-(2-hydroxy-2-phenylethyl)-1,5-dihydro-4*H*-pyrazolo[3,4-*d*]pyrimidin-4-one **14** (346 mg, 1 mmol) in $CHCl_3$ (10 mL). The mixture was refluxed for 12 h. The solution was washed with water (2 × 20 mL), dried ($MgSO_4$), filtered, and concentrated under reduced pressure. The crude oil was purified by column chromatography (Florisil, 100–200 mesh), using diethyl ether as the eluent, to afford the compound as a yellow oil, which crystallized standing in a refrigerator by adding a 1:1 mixture of Et_2O/PE (bp 40–60 °C). White solid (320 mg, 84%); mp 172–173 °C. ^{1}H NMR: δ 3.99 (s, 2H, CH_2Ar), 4.64–4.77 and 4.81–4.96 (2m, 2H, CH_2N), 5.36–5.51 (m, 1H, CHCl), 7.03–7.66 (m, 10H Ar), 8.03 (s, 1H, H-3). MS: m/z $[M + 1]^+$ 384. Anal. ($C_{20}H_{16}N_4Cl_2$) C, H, N.

General Procedure for the Synthesis of 17a–e. A 60% sodium hydride dispersion in mineral oil (1.21 g, 30.3 mmol) was added in small batches to a solution of malonitrile **16** (1.00 g, 15.1 mmol) in dry THF (25 mL) precooled at 0–5 °C. After 30 min at 0–5 °C, the suitable acyl chloride (15.1 mmol) was added dropwise. The orange solution was stirred at room temperature for 2–12 h, then dimethylsulfate (1.75 mL, 18.2 mmol) was slowly added and the solution was refluxed for 3–6 h. Finally, 2-hydrazino-1-phenylethanol **11** (4.62 g, 30.2 mmol) dissolved in dry THF (2 mL) was added and the reaction was refluxed for 3–6 h. After cooling to room temperature, water (25 mL) and conc NH_3 (5 mL) were added under stirring. After 15 min, THF was removed under reduced pressure and the aqueous phase was extracted with CH_2Cl_2 (3 × 30 mL). Organic phases were washed with water (15 mL) and brine (15 mL), dried (Na_2SO_4), and evaporated under reduced pressure. The crude was purified by flash chromatography (silica gel 0.060–0.200 mm, 40 Å) using Et_2O/PE (bp 40–60 °C) as the eluent, with a gradient eluition (3:1 → 9:1) to afford compounds **17a–e**.

*5-Amino-1-(2-hydroxy-2-phenylethyl)-3-phenyl-1H-pyrazole-4-carbonitrile (**17a**).* White solid (1.84 g, 40%); mp 165–166 °C. ^{1}H NMR: δ 3.95–4.23 (m, 2H, CH_2), 5.10–5.18 (m, 1H, CH), 7.20–7.37 and 7.79–7.81 (2m, 10H Ar). IR (cm^{-1}): 3560–3240 (OH), 3358, 3350 (NH_2), 2204 (CN). MS: m/z 305 $[M+1]^+$. Anal. ($C_{18}H_{16}N_4O$) C, H, N.

*5-Amino-3-(4-fluorophenyl)-1-(2-hydroxy-2-phenylethyl)-1H-pyrazole-4-carbonitrile (**17b**).* White solid (1.54 g, 32%); mp 175–176 °C. ^{1}H NMR: δ 4.01–4.10 and 4.15–4.19 (2m, 2H, CH_2), 5.12–5.18 (m, 1H, CH), 7.19–7.52 and 8.25–8.30 (2m, 9H Ar). IR (cm^{-1}): 3450–2900 (OH), 3388, 3323 (NH_2), 2223 (CN). MS: m/z 323 $[M+1]^+$. Anal. ($C_{18}H_{15}N_4FO$) C, H, N.

*5-Amino-3-(4-chlorophenyl)-1-(2-hydroxy-2-phenylethyl)-1H-pyrazole-4-carbonitrile (**17c**).* White solid (2.50 g, 49%); mp 173–174 °C. ^{1}H NMR: δ 3.99–4.15 (m, 2H, CH_2), 5.12–5.18 (m, 1H, CH), 7.50–7.54 and 7.96–7.99 (2m, 9H Ar). IR (cm^{-1}): 3450–3100 (OH), 3388, 3322 (NH_2), 2223 (CN). MS: m/z 340 $[M+1]^+$. Anal. ($C_{18}H_{15}N_4ClO$) C, H, N.

*5-Amino-1-(2-hydroxy-2-phenylethyl)-3-(4-methylphenyl)-1H-pyrazole-4-carbonitrile (**17d**).* White solid (2.02 g, 42%); mp 172–174 °C. ^{1}H NMR: δ 2.36 (s, 3H, CH_3), 4.00–4.05 and 4.12–4.15 (2m, 2H, CH_2), 5.10–5.15 (m, 1H, CH), 7.20–7.34 and 7.57–7.91 (2m, 9H Ar). IR (cm^{-1}): 3400–3200 (OH), 3400, 3322 (NH_2), 2221 (CN). MS: m/z 319 $[M+1]^+$. Anal. ($C_{19}H_{18}N_4O$) C, H, N.

*5-Amino-1-(2-hydroxy-2-phenylethyl)-3-(4-methoxyphenyl)-1H-pyrazole-4-carbonitrile (**17e**).* White solid (2.50 g, 50%); mp 144–145 °C. ^{1}H NMR: δ 3.79 (s, 3H, CH_3), 4.03–4.06 and 4.10–4.15 (2m, 2H, CH_2), 5.11–5.15 (m, 1H, CH), 7.18–7.30 and 7.60–7.85 (2m, 9H Ar). IR (cm^{-1}): 3450–2900 (OH), 3409, 3351 (NH_2), 2220 (CN). MS: m/z 335 $[M+1]^+$. Anal. ($C_{19}H_{18}N_4O_2$) C, H, N.

General Procedure for the Synthesis of 18a–e. A suspension of the suitable intermediate **17a–e** (3 mmol) in formamide (18 mL, 450 mmol) was heated at 190 °C for 3–4 h and then poured into water (40 mL). The crude solid was filtered, washed with water, suspended in ethanol, and boiled with charcoal for 10 min. The solid dissolved at the ethanol boiling point. After charcoal filtration, compounds **18a**, **18c**, and **18d** precipitated as pure solids. Compounds **18b** and **18e** were further purified by flash chromatography (silica gel 0.060–0.200 mm, 40 Å) using CH_2Cl_2/CH_3OH (98:2) as the eluent to afford pure oils that slowly crystallized by adding a 1:1 mixture of Et_2O/PE (bp 40–60 °C).

*2-(4-Amino-3-phenyl-1H-pyrazolo[3,4-d]pyrimidin-1-yl)-1-phenylethanol (**18a**).* White solid (549 mg, 55%); mp 160–161 °C. ^{1}H NMR: δ 4.10–4.32 and 4.40–4.38 (2m, 2H, CH_2), 5.02–5.08 (m, 1H, CH), 7.16–7.22 and 7.42–7.50 (2m, 10H Ar), 8.09 (s, 1H, H-6). IR (cm^{-1}): 3500–2900 (OH), 3474, 3315 (NH_2). MS: m/z 332 $[M + 1]^+$. Anal. ($C_{19}H_{17}N_5O$) C, H, N.

*2-[4-Amino-3-(4-fluorophenyl)-1H-pyrazolo[3,4-d]pyrimidin-1-yl]-1-phenylethanol (**18b**).* White solid (497 mg, 48%); mp 190–192 °C. ^{1}H NMR: δ 4.12–4.34 and 4.42–4.45 (2m, 2H, CH_2), 5.05–5.10 (m, 1H, CH), 7.19–7.30 and 7.51–7.60 (2m, 9H Ar), 8.12 (s, 1H, H-6). IR (cm^{-1}): 3500–3060 (OH), 3484, 3307 (NH_2). MS: m/z 350 $[M + 1]^+$. Anal. ($C_{19}H_{16}N_5FO$) C, H, N.

*2-[4-Amino-3-(4-chlorophenyl)-1H-pyrazolo[3,4-d]pyrimidin-1-yl]-1-phenylethanol (**18c**).* White solid (509 mg, 46%); mp 200–201 °C. ^{1}H NMR: δ 4.21–4.28 and 4.35–4.42 (2m, 2H, CH_2), 5.15–5.18 (m, 1H, CH), 7.21–7.34 and 7.70–7.82 (2m, 9H Ar), 8.10 (s, 1H, H-6). IR (cm^{-1}): 3450–2990 (OH), 3407, 3290 (NH_2). MS: m/z 367 $[M + 1]^+$. Anal. ($C_{19}H_{16}N_5ClO$) C, H, N.

*2-[4-Amino-3-(4-methylphenyl)-1H-pyrazolo[3,4-d]pyrimidin-1-yl]-1-phenylethanol (**18d**).* White solid (496 mg, 48%); mp 93–95 °C. ^{1}H NMR: δ 2.37 (s, 3H, CH_3), 4.20–4.25 and 4.30–4.37 (2m, 2H, CH_2), 5.10–5.15 (m, 1H, CH), 7.19–7.32 and 7.50–7.78 (2m, 9H Ar), 8.12 (s, 1H, H-6). IR (cm^{-1}): 3500–3000 (OH), 3469, 3296 (NH_2). MS: m/z 346 $[M + 1]^+$. Anal. ($C_{20}H_{19}N_5O$) C, H, N.

*2-[4-Amino-3-(4-methoxyphenyl)-1H-pyrazolo[3,4-d]pyrimidin-1-yl]-1-phenylethanol (**18e**).* White solid (427 mg, 39%); mp 161–163 °C. ^{1}H NMR: δ 3.82 (s, 3H, CH_3), 4.22–4.27 and 4.33–4.41

DOI: 10.1021/acs.jmedchem.5b00140
J. Med. Chem. 2015, 58, 4590–4609

(2m, 2H, CH_2), 5.13−5.21 (m, 1H, CH), 7.15−7.38 and 7.45−7.90 (2m, 9H Ar), 8.10 (s, 1H, H-6). IR (cm^{-1}): 3500−2900 (OH), 3461, 3360 (NH_2). MS: m/z 362 $[M + 1]^+$. Anal. ($C_{20}H_{19}N_5O_2$) C, H, N.

1*H*-Pyrazolo[3,4-*d*]pyrimidin-4-amine (22). A solution of 5-amino-1*H*-pyrazolo-4-carbonitrile **21** (400 mg, 3.7 mmol) and formamide (5 mL, 125.8 mmol) was stirred at 200 °C for 1 h. After cooling to room temperature, water was added (20 mL) and the obtained solid was filtered. The crude product was suspended in hot water (40 mL) and conc HCl (5 mL), then charcoal (600 mg) was added and the mixture was boiled for 15 min. After charcoal filtration, conc NH_3 was added and the precipitated solid was filtered, giving compound **22** as a white solid (405 mg, 81%); mp 353−356 °C (Lit. 58%, mp >300 °C).[42,43,66]

3-Iodo-1*H*-pyrazolo[3,4-*d*]pyrimidin-4-amine (23). *N*-iodosuccinimide (2 g, 8.9 mmol) was added to a solution of 1*H*-pyrazolo[3,4-*d*]pyrimidin-4-amine **22** (800 mg, 5.9 mmol) in dry DMF (5 mL) and the mixture heated at 80 °C for 14 h under nitrogen atmosphere. After cooling to room temperature, water was added (20 mL) and the precipitated solid was filtered and washed with water (50 mL). The crude product was recrystallized from absolute ethanol to give compound **23** as a light-yellow solid (1.31 g, 85%); mp 272−275 °C.[43]

3-Iodo-1-(2-phenylpropyl)-1*H*-pyrazolo[3,4-*d*]pyrimidin-4-amine (24). K_2CO_3 (600 mg, 4.34 mmol) was added to a solution of 3-iodo-1*H*-pyrazolo[3,4-*d*]pyrimidin-4-amine **23** (400 mg, 1.53 mmol) in dry DMF (5 mL), and the mixture was heated at 50 °C for 1 h. 1-Bromo-2-phenylpropane (350 μL, 2.30 mmol) was added, and the reaction was stirred at 130 °C for 18 h. After cooling to room temperature, water was added (30 mL) and the precipitated solid was filtered and purified by column chromatography (silica gel 0.060−0.200 mm, 40 Å) using a mixture of CH_2Cl_2/MeOH (95:5) as the eluent to afford compound **24** as a white solid (390 mg, 67%); mp 265−268 °C. ^{1}H NMR: δ 1.22 (m, 3H, CH_3), 3.52−3.57 (m, 1H, CH), 4.48−4.50 (m, 2H, CH_2), 5.83 (br s, 2H, NH_2 disappears with D_2O), 7.18−7.28 (m, 5H Ar), 8.28 (s, 1H, H-6). IR (cm^{-1}): 3480, 3360 (NH_2). MS: m/z 380 $[M + H]^+$. Anal. ($C_{14}H_{14}N_5I$) C, H, N.

2-(Methylthio)pyrimidine-4,6-diol (26). A mixture of KOH (5.00 g, 38.2 mmol), H_2O (50 mL), thiobarbituric acid **25** (5.0 g, 34.7 mmol), and CH_3I (2.4 mL, 38.2 mmol) was stirred at reflux for 3 h. The solution was allowed to cool to room temperature, then acidified with 3 N HCl until pH ∼ 2. The product was obtained by filtration. Pale-yellow solid (4.67 g, 87%); mp 98−99 °C. ^{1}H NMR: δ 2.54 (s, 3H, SCH_3), 4.86 (br s, 1H, OH, disappears with D_2O), 5.24 (s, 1H, H-5). MS: m/z $[M - 1]^-$ 157. Anal. ($C_5H_6N_2O_2S$) C, H, N, S.

4,6-Dichloro-2-(methylthio)pyrimidine (27). 2-(Methylthio)-pyrimidine-4,6-diol **26** (1.0 g, 6.3 mmol) was added to freshly distilled $POCl_3$ (4.40 mL, 47.5 mmol). The mixture was stirred at reflux under nitrogen atmosphere, then, once cooled to room temperature, H_2O (50 mL) was added and the suspension was stirred at room temperature for 12 h. After this time, extraction with EtOAc (3 × 50 mL) was performed, the collected organic phases were dried $(Na_2SO)_4$ and filtered, and the solvent removed under reduced pressure. The yellow oily residue obtained was purified by flash chromatography (Hex/EtOAc, 99:1) to afford the product as a light-yellow oil. Light yellow oil (494 mg, 40%). ^{1}H NMR: δ 2.57 (s, 3H, SCH_3), 6.89 (s, 1H, H-5). MS: m/z $[M + 1]^+$ 196. Anal. ($C_5H_4N_2Cl_2S$) C, H, N, S.

4,6-Dichloro-2-(methylthio)pyrimidin-5-yl)(phenyl)-methanol (28). A 2 M solution of LDA (695 μL, 1.39 mmol) was added dropwise to a solution of 4,6-dichloro-2-(methylthio)pyrimidine **27** (150.0 mg, 0.77 mmol) in anhydrous THF (2 mL) at −78 °C. The mixture was stirred at the same temperature for 30 min, then benzaldehyde (118.4 μL, 1.16 mmol) in anhydrous THF (2 mL) was added dropwise at room temperature and the resulting mixture was stirred for 1 h. NH_4Cl saturated solution was added, and the aqueous phase was extracted twice with EtOAc (3 × 20 mL). The collected organic phases were dried (Na_2SO_4) and filtered and the solvent evaporated under reduced pressure. The oily residue obtained was purified by flash chromatography, using PE/EtOAc (98:2) as the eluent. Light-brown solid (162 mg, 70%); mp 87−88 °C. ^{1}H NMR: δ 2.56 (s, 3H, SCH_3), 6.48 (s, 1H, CHOH), 7.18−7.41 (m, 5H, Ar). MS: m/z $[M - 1]^-$ 300. Anal. ($C_{12}H_{10}N_2Cl_2OS$) C, H, N, S.

(4,6-Dichloro-2-(methylthio)pyrimidin-5-yl)(phenyl)-methanone (29). In a flask equipped with a Dean−Stark trap, a mixture of the secondary alcohol **28** (150 mg, 0.50 mmol), toluene (10 mL), and MnO_2 (215.3 mg, 2.5 mmol) was boiled for 1 h. The mixture was filtered on Celite using EtOAc. The organic phase was dried (Na_2SO_4) and filtered and the solvent evaporated under reduced pressure to obtain the product used without further purification in the next step. White solid (89.7 mg, 60%); mp 102−103 °C. ^{1}H NMR: δ 2.62 (s, 3H, SCH_3), 7.50−7.54 (t, J = 7.6 Hz, 2H, Ar), 7.65−7.69 (t, J = 7.6 Hz, 1H, Ar), 7.82−7.86 (d, J = 7.6 Hz, 2H, Ar). Anal. ($C_{12}H_8N_2Cl_2OS$) C, H, N, S.

4-Chloro-6-(methylthio)-3-phenyl-1*H*-pyrazolo[3,4-*d*]-pyrimidine (30). To an ice-cooled solution of the appropriate ketone **29** (134 mg, 0.45 mmol) and TEA (62.8 μL, 0.45 mmol) in dioxane was added hydrazine monohydrate (24 μL, 0.50 mmol). After 5 min, the ice bath was removed and the reaction mixture was stirred at room temperature for 5 h. After this time, 0.5 N HCl (10 mL) was added and the solution was extracted with EtOAc (3 × 20 mL). The collected organic phases were dried (Na_2SO_4) and filtered and the solvent removed under reduced pressure to afford the desired product that was used in the next step without further purification. Light-yellow solid (124 mg, quant.); mp 107−108 °C. ^{1}H NMR: δ 2.63 (s, 3H, SCH_3), 7.45−7.50 (m, 3H Ar), 7.69−7.75 (m, 2H, Ar). Anal. ($C_{12}H_9ClN_4S$) C, H, N, S.

General Procedure for the Synthesis of 31a,b. To an ice-cooled solution of Ph_3P (70.8 mg, 0.27 mmol) and 4-chloro-6-(methylthio)-3-phenyl-1*H*-pyrazolo[3,4-*d*]pyrimidine **30** (50 mg, 0.18 mmol) in anhydrous THF (2 mL) was added the appropriate 2-phenylethanol (0.18 mmol), followed by dropwise addition of DIAD (53.2 μL, 0.27 mmol). The reaction mixture was stirred at 4 °C for 15 min, and then allowed to warm to room temperature. The reaction was irradiated under MW at 100 °C for 3 min; after evaporation of the solvent, the oily residue obtained was purified by flash chromatography using PE/EtOAc (95:5) as the eluent.

*4-Chloro-6-(methylthio)-1-phenethyl-3-phenyl-1H-pyrazolo[3,4-d]pyrimidine (**31a**).* White solid (49.5 mg, 72%); mp 95−96 °C. ^{1}H NMR: δ 2.60 (s, 3H, SCH_3), 3.26−3.30 (t, J = 7.6 Hz, 2H, CH_2), 4.68−4.72 (t, J = 7.6 Hz, 2H, CH_2), 7.17−7.28 (m, 5H Ar), 7.48−7.51 (m, 3H, Ar), 7.74−7.76 (m, 2H, Ar). Anal. ($C_{20}H_{17}ClN_4S$) C, H, N, S.

*4-Chloro-1-(2-methoxy-2-phenylethyl)-6-(methylthio)-3-phenyl-1H-pyrazolo[3,4-d]pyrimidine (**31b**).* White solid (51 mg, 69%); mp 97−98 °C. ^{1}H NMR: δ 2.61 (s, 3H, SCH_3), 3.22 (s, 3H, OCH_3), 4.49−4.51 and 4.78−4.84 (m, 2H, CH_2), 4.89−4.92 (m, 1H, CH), 7.29−7.34 (m, 5H Ar), 7.48−7.49 (m, 3H, Ar), 7.76−7.78 (m, 2H, Ar). Anal. ($C_{21}H_{19}ClN_4OS$) C, H, N, S.

Biology. *Enzymatic Assay on Isolated Fyn Kinase.* Active, recombinant Fyn and the specific peptide substrates (Src Substrate Peptide, cat. 12-140) were purchased from Merck-Millipore. Kinase assays were performed in the presence of 200 μM ATP and 100 μM peptide substrate. All inhibition assays were conducted with 0.01 μg of active kinase, 0.33 pmol [γ^{32}P]ATP, 60 mM HEPES−NaOH, pH 7.5, 3 μM Na-orthovanadate, 1.2 mM DTT, 50 μg/mL $PEG_{20.000}$, 10 mM magnesium acetate, 0.004%NP40, and 10% DMSO in a final volume of 10 μL. Fyn and inhibitors were preincubated in ice for 5 min; after addition of the substrates, the reaction was conducted at 30 °C for 10 min. The reaction was stopped by adding 5 μL of 3% phosphoric acid. Aliquots (10 μL) were then transferred into a P30 Filtermat (PerkinElmer) and washed five times with 75 mM phosphoric acid and once with acetone for 5 min. The filter was dried and transferred to a sealable plastic bag, and scintillation cocktail (4 mL) was added. Spotted reactions were read in a MicroBeta Liquid (PerkinElmer) scintillation counter. The ID_{50} values were obtained according to the following equation:

$$\nu = V/(1 + (I/ID_{50})$$

where ν is the measured reaction velocity, V is the apparent maximal velocity in the absence of inhibitor, I is the inhibitor concentration, and the ID_{50} is the 50% inhibitory dose.

DOI: 10.1021/acs.jmedchem.5b00140
J. Med. Chem. 2015, 58, 4590−4609

K_i values toward recombinant Fyn were calculated using the equation:

$$K_i = (ID_{50}/(1 + K_{mATP}/[S_{ATP}]))$$

according to a competitive mechanism of inhibition toward ATP substrate, where $[S_{ATP}]$ is the concentration of ATP. Curve fitting was performed with the program GraphPad Prism version 5.00.

Cell Culture, Differentiation, and Treatments on SH-SY5Y Cells. The neuroblastoma cell line SH-SY5Y was cultured in media obtained by mixing equal volume of MEM and HAM F12 supplemented with 15% fetal calf serum (FCS, Australian origin, Lonza), 100U/mL penicillin, 100 μg/mL streptomycin, and 2 mM L-glutamine (all from Euroclone) at 37 °C in humidified air with 5% CO_2. The medium was changed every 48 h. Cells were split at about 80% confluence and never cultured beyond passage 20. Cell differentiation was achieved by pretreating for 5 days the SH-SY5Y cells with media containing 1% FCS and 10 μM retinoic acid (RA, Sigma-Aldrich). Subsequently, cells were treated for other 7 days in media with no serum and supplemented with 50 ng/mL of human recombinant brain derived neurotrophic factor (BDNF, Peprotech), 10 ng/mL human recombinant beta nerve growth factor (NGF, Peprotech), 10 ng/mL neuregulin 1 beta 2 protein (NRG, Abcam), and 9.35 μg/mL vitamin D3 (Sigma-Aldrich). To confirm full neuronal differentiation, the expression of mature isoforms of Tau were checked.[46] Differentiated cells were treated for 1.5, 3, and 6 h with media containing 10 μM $A\beta_{42}$ oligomer/protofibrils and N2 supplement (Life Technologies) in the presence or in the absence of Fyn inhibitors dissolved in DMSO. As control, cells were treated with media containing equivalent amounts of DMSO.

$A\beta_{42}$ Preparation. $A\beta_{42}$ oligomer/protofibril samples were prepared using previously described protocols.[48] Briefly, $A\beta_{42}$ peptides (Sigma) were dissolved in 1,1,1,3,3,3-hexafluoro-2-propanol and lyophilized to completely remove the solvent. Lyophilized $A\beta_{42}$ peptides were reconstituted in DMSO to a working concentration of 10 mM, diluted 1:100 using HAM F12 (without phenol red and glutammine), vortexed for 15 s, and incubated 24 h at 4 °C. $A\beta_{42}$ oligomer/protofibrils were visualized by SDS-PAGE and silver staining.

Antiproliferative Activity on Human Cell Line K562. In vitro experiments were carried out using the human CML cell line K562. Cells were purchased from American Type Culture Collection (ATCC, Manassas, VA, USA) and were cultured in RPMI medium supplemented with 10% fetal bovine serum. To determine antiproliferative effect of Fyn inhibitors, K562 cells were seeded at 2×10^5 cells/mL density and treated with compounds at increasing concentrations from 0.01 to 50 μM. The cultures were maintained at 37 °C in 5% v/v CO_2 for 72 h. Cell number and vitality were evaluated using the automatic cell counter NucleoCounter (Chemometec, Denmark). Results from the NucleoCounter represented either total or nonviable cell concentration, depending on the sample preparation indicated by manufacturer. IC_{50} (drug concentration that determined the 50% of growth inhibition) was calculated by Grafit v4.0 (Erithacus Software Limited) software using the best fitting sigmoid curve.

Cell Cycle Analysis. Exponential growing cells were treated with selected inhibitors at the density of 1×10^6 cells/mL for 48 h. At the end point, at least 5×10^6 cells were harvested, washed with phosphate buffer saline (PBS), and fixed overnight with 70% ethanol. Then, ethanol was removed by centrifugation and the cells resuspended in PBS, stained with the 50 μg/mL propidium iodide (PI) at 4 °C for 30 min in the dark. Stained cells were analyzed by Tali image-based cytometer (Life Technologies, Carlsbad, CA, USA) counting 20 fields for sample, and exported fcs raw data were elaborated by Flowing software (v. 2.5.0, by Perttu Terho, University of Turku, Finland).

Apoptosis Assay on CD34+ from CML Patients. A 46-year-old woman who did not respond to treatment with Imatinib (400 mg/die) and Dasatinib (140 mg/die) was selected for the test on Ph+ CML patient. A bone marrow sample was collected after informed consent. Mononuclear cells were isolated by density gradient centrifugation in Ficoll−Hypaque and resuspended in RPMI medium with 10% FBS. Cells were seeded 2×10^5 cells/mL density and treated with Imatinib 1 μM and with **4c−d** 2 μM for 48 h. After incubation time, cells were harvested and labeled for 15 min with antibodies against human CD34 and CD45 (APC Mouse Anti-Human CD34 and PerCP Mouse Anti-Human CD45, BD Pharmingen). To determine apoptotic effects of compounds, cells were washed with phosphate buffered saline (PBS), resuspended in annexin buffer, and labeled for 15 min with Annexin V-FITC/propidium iodide (PI) (FITC Annexin V apoptosis detection kit II, BD Pharmingen). At least 150000 events were analyzed using BD FACSCalibur flow cytometer.

Time-Dependent Cell Response Profiling Using the Real-Time RTCA iCELLigence System. The RTCA iCELLigence system is a microelectronic biosensor system for cell-based assay. Cell viability, cell number, cell morphology, and degree of adhesion were evaluated by real-time electrode impedance. A dimensionless parameter termed Cell Index (CI) was used to measure the relative change in electrical impedance and to quantify cell status. The evaluation of cell viability was performed on MDA-MB-231 and U87 cell lines according to previous descriptions.[67]

MDA-MB-231, human breast cancer cell line, and U87, human glioblastoma multiforme cell line, were purchased from ATCC and cultured according to provider's indication. For time-dependent cell response profiling, 150 μL of media was added to 8-well electric plates (E-Plates) to obtain background readings followed by the addition of 300 μL of cell suspension at the density of 35000 cells/mL. The E-plates containing the cells were allowed to incubate at room temperature for 30 min and placed on the reader in the incubator for continuous recording of impedance as reflected by CI. After 20−24 h, the cells were treated with different dilutions of the compounds. Each compound dilution plate also contained DMSO only diluted wells as well as media only wells. The cells were monitored every 2 min for duration of 1 h after compound addition to capture the short-term response and for every 15 min from 1 h after compound addition to about 100 h to capture the long-term response. A "Normalized Cell Index" at a given time point, just prior to the treatment, was calculated by dividing the CI at the time point by the CI at a reference time point. Thus, the Normalized Cell Index is 1 at the reference time point. The IC_{50} was calculated by RTCA data analysis software using the best fit of a sigmoidal dose−response (variable slope) curve form at least three different dilutions of the compounds.

ADME Assay. *Chemicals.* All solvents and reagents were from Sigma-Aldrich Srl (Milan, Italy) and Brain Polar Lipid Extract (Porcine) was from Avanti Polar Lipids, Inc. (Alabama, USA). Dodecane was purchased from Fluka (Milan, Italy). Pooled Male Donors 20 mg/mL HLM were from BD Gentest-Biosciences (San Jose, California). Milli-Q quality water (Millipore, Milford, MA, USA) was used. Hydrophobic filter plates (MultiScreen-IP, Clear Plates, 0.45 μm diameter pore size), 96-well microplates, and 96-well UV-transparent microplates were obtained from Millipore (Bedford, MA, USA).

Parallel Artificial Membrane Permeability Assay (PAMPA and PAMPA-BBB). Donor solution (0.5 mM) was prepared by diluting 1 mM dimethyl sulfoxide (DMSO) compound stock solution using phosphate buffer (pH 7.4, 0.025 M). Filters were coated with 5 μL of a 1% (w/v) dodecane solution of phosphatidylcholine or 4 μL of brain polar lipid solution (20 mg/mL 16% $CHCl_3$, 84% dodecane) prepared from $CHCl_3$ solution 10% w/v, for intestinal permeability and BBB permeability, respectively. Donor solution (150 μL) was added to each well of the filter plate. To each well of the acceptor plate were added 300 μL of solution (50% DMSO in phosphate buffer). All compounds were tested in three different plates on different days. The sandwich was incubated for 5 h at room temperature under gentle shaking. After the incubation time, the plates were separated and samples were taken from both receiver and donor sides and analyzed using LC with UV detection at 280 nm. LC analysis were performed with a PerkinElmer (series 200) instrument equipped with an UV detector (PerkinElmer 785A, UV/vis Detector). Chromatographic separations were conducted using a Polaris C18 column (150−4.6 mm, 5 μm particle size) at a flow rate of 0.8 mL min^{-1} with a mobile phase composed of 60% ACN/40% H_2O−formic acid 0.1% for all compounds. Permeability (P_{app}) for PAMPA and PAMPA-BBB were calculated according to the following equation, obtained from the Wohnsland and Faller[68] and

DOI: 10.1021/acs.jmedchem.5b00140
J. Med. Chem. 2015, 58, 4590−4609

Sugano et al.[69] equation with some modification in order to obtain permeability values in cm/s,

$$Papp = \frac{V_D V_A}{(V_D + V_A)At} - \ln(1 - r)$$

where V_A is the volume in the acceptor well, V_D is the volume in the donor well (cm^3), A is the "effective area" of the membrane (cm^2), t is the incubation time(s), and r the ratio between drug concentration in the acceptor and equilibrium concentration of the drug in the total volume ($V_D + V_A$). Drug concentration is estimated by using the peak area integration. Membrane retentions (%) were calculated according to the following equation:

$$\%MR = \frac{[r - (D + A)]100}{Eq}$$

where r is the ratio between drug concentration in the acceptor and equilibrium concentration, D, A, and Eq represent drug concentration in the donor, acceptor, and equilibrium solution, respectively.

Water Solubility Assay. Each solid compound (1 mg) was added to 1 mL of water. The samples were shaked in a shaker bath at room temperature for 24−36 h. The suspensions were filtered through a 0.45 μm nylon filter (Acrodisc), and the solubilized compound determined by LC-MS-MS assay. For each compound, the determination was performed in triplicate. For the quantification an LC-MS system was used consisting of a Varian apparatus (Varian Inc.) including a vacuum solvent degassing unit, two pumps (212-LC), a triple quadrupole MSD (model 320-LC) mass spectrometer with ES interface and Varian MS Workstation System Control version 6.9 software. Chromatographic separation was obtained using a Pursuit C18 column (50 mm × 2.0 mm) (Varian) with 3 μm particle size and gradient elution: eluent A being ACN and eluent B consisting of an aqueous solution of formic acid (0.1%). The analysis started with 0% of eluent A, which was linearly increased up to 70% in 10 min, then slowly increased up to 98% up to 15 min. The flow rate was 0.3 mL/min and injection volume was 5 μL. The instrument operated in positive mode and parameters were: detector 1850 V, drying gas pressure 25.0 psi, desolvation temperature 300.0 °C, nebulizing gas 45.0 psi, needle 5000 V, and shield 600 V. Nitrogen was used as nebulizer gas and drying gas. Collision induced dissociation was performed using Argon as the collision gas at a pressure of 1.8 mTorr in the collision cell. The transitions as well as the capillary voltage, and the collision energy used for compound are summarized in Table 1S (Supporting Information). Quantification of the single compound was made by comparison with apposite calibration curves realized with standard solutions in methanol.

Microsomal Stability Assay. Each compound in DMSO solution was incubated at 37 °C for 60 min in 125 mM phosphate buffer (pH 7.4), 5 μL of human liver microsomal protein (0.2 mg/mL), in the presence of a NADPH-generating system at a final volume of 0.5 mL (compounds' final concentration, 50 μM); DMSO did not exceed 2% (final solution). The reaction was stopped by cooling in ice and adding 1.0 mL of acetonitrile. The reaction mixtures were then centrifuged, and the parent drug and metabolites were subsequently determined by LC-UV-MS. Chromatographic analysis were performed with an Agilent 1100 LC/MSD VL system (G1946C) (Agilent Technologies, Palo Alto, CA) constituted by a vacuum solvent degassing unit, a binary high-pressure gradient pump, an 1100 series UV detector, and an 1100 MSD model VL benchtop mass spectrometer. Chromatographic separation was obtained using a Varian Polaris C18-A column (150−4.6 mm, 5 μm particle size) and gradient elution: eluent A being ACN and eluent B consisting of an aqueous solution of formic acid (0.1%). The analysis started with 2% of eluent A, which was rapidly increased up to 70% in 12 min, then slowly increased up to 98% in 20 min. The flow rate was 0.8 mL min^{-1}, and injection volume was 20 μL. The Agilent 1100 series mass spectra detection (MSD) single-quadrupole instrument was equipped with the orthogonal spray API-ES (Agilent Technologies, Palo Alto, CA). Nitrogen was used as nebulizing and drying gas. The pressure of the nebulizing gas, the flow of the drying gas, the capillary voltage, the fragmentor voltage, and the vaporization temperature were set at 40 psi, 9 L/min, 3000 V, 70 V, and 350 °C, respectively. UV detection was monitored at 280 nm. The LC-ESI-MS determination was performed by operating the MSD in the positive ion mode. Spectra were acquired over the scan range m/z 100−1500 using a step size of 0.1 μ. The percentage of not metabolized compound was calculated by comparison with reference solutions.

■ ASSOCIATED CONTENT

Supporting Information

A table with elemental analysis for compounds **3j−o**, **4a−e**, **5a−e**, **8b**, **9b**, **12**, **14**, **15**, **17a−e**, **18a−e**, **22−24**, **26−30**, **31a,b** and **6a,b**, and a table with chromatographic and MS parameters. The Supporting Information is available free of charge on the ACS Publications website at DOI: 10.1021/acs.jmedchem.5b00140.

■ AUTHOR INFORMATION

Corresponding Authors

*For S.S.: phone, (+39)010-3538866; fax, (+39)010 3538358; E-mail, schensil@unige.it.

*For E.C.: phone, (+39) 0382-546355; fax, (+39) 0382-422286; E-mail, crespan@igm.cnr.it.

Present Addresses

¶For M.R.: Dipartimento di Farmacia, University of Parma, Parco Area delle Scienze 27/A, Parma 43124, Italy.

⁺For F.F.: Department of Pharmacy and Biotechnology, University of Bologna, Via Belmeloro 6, 40126 Bologna, Italy; Department of Drug Discovery and Development, Italian Institute of Technology, Via Morego 30, 16163 Genova, Italy.

Notes

The authors declare no competing financial interest.

■ ACKNOWLEDGMENTS

This work was partially supported by the Italian Association for Cancer Research AIRC IG_4538 and National Interest Research Projects (2010W2KM5L_007) grants to G.M., and by National Interest Research Projects (PRIN_2007_N7-KYCY) to G.M., M.B., and S.S. (PRIN_2008_5HR5JK). Financial support has been also received from the Istituto Toscano Tumori-ITT-Grant proposal 2010. S.S. was also supported by the National Interest Research Project PRIN_2010_5YY2HL. Rottapharm is also acknowledged for financial support. We are grateful to Lead Discovery Siena Srl and Cost Action CM1106 "Chemical Approaches to Targeting Drug Resistance in Cancer Stem Cells". Work in authors' laboratories was partially supported by "Progetto di interesse invecchiamento MIUR-CNR". M.G. and A.L. were supported by "Progetto di interesse invecchiamento MIUR-CNR" fellowship. We are indebted to Molecular Discovery for access to the Metasite software. Special thanks to Giulio Parrella for his degree thesis.

■ ABBREVIATIONS USED

SFKs, Src family kinases; AD, Alzheimer's disease; CNS, central nervous system; CML, chronic myeloid leukemia; MD, molecular dynamics; RMSD, root-mean-square deviation; RMSFs, root-mean-square fluctuations; MM-PB/GBSA, molecular mechanics Poisson−Boltzmann/generalized Born surface area; PAMPA, parallel artificial membrane permeability assay; BBB, blood−brain barrier

DOI: 10.1021/acs.jmedchem.5b00140
J. Med. Chem. 2015, 58, 4590−4609

REFERENCES

(1) Brown, M. T.; Cooper, J. A. Regulation, substrates and functions of src. *Biochim. Biophys. Acta* **1996**, *1287*, 121−149.
(2) Goldsmith, J. F.; Hall, C. G.; Atkinson, T. P. Identification of an alternatively spliced isoform of the Fyn tyrosine kinase. *Biochem. Biophys. Res. Commun.* **2002**, *298*, 501−504.
(3) Thomas, S. M.; Brugge, J. S. Cellular functions regulated by Src family kinases. *Annu. Rev. Cell Dev. Biol.* **1997**, *13*, 513−609.
(4) Hanks, S. K.; Quinn, A. M.; Hunter, T. The protein kinase family: conserved features and deduced phylogeny of the catalytic domains. *Science* **1988**, *241*, 42−52.
(5) Rybin, V. O.; Guo, J.; Gertsberg, Z.; Feinmark, S. J.; Steinberg, S. F. Phorbol 12-myristate 13-acetate-dependent protein kinase C delta-Tyr311 phosphorylation in cardiomyocyte caveolae. *J. Biol. Chem.* **2008**, *283*, 17777−17788.
(6) Salmond, R. J.; Filby, A.; Qureshi, I.; Caserta, S.; Zamoyska, R. T cell receptor proximal signaling via the Src-family kinases, Lck and Fyn, influences T-cell activation, differentiation, and tolerance. *Immunol. Rev.* **2009**, *228*, 9−22.
(7) Levi, M.; Shalgi, R. The role of Fyn kinase in the release from metaphase in mammalian oocytes. *Mol. Cell. Endocrinol.* **2010**, *314*, 228−233.
(8) Vatish, M.; Yamada, E.; Pessin, J. E.; Bastie, C. C. Fyn kinase function in lipid utilization: a new upstream regulator of AMPK activity? *Arch. Physiol. Biochem.* **2009**, *115*, 191−198.
(9) Kopeć, A.; Panaszek, B.; Fal, A. M. Intracellular signaling pathways in IgE-dependent mast cell activation. *Arch. Immunol. Ther. Exp.* **2006**, *54*, 393−401.
(10) Schenone, S.; Brullo, C.; Musumeci, F.; Biava, M.; Falchi, F.; Botta, M. Fyn kinase in brain diseases and cancer; the search for inhibitors. *Curr. Med. Chem.* **2001**, *18*, 2921−2942.
(11) Lee, G. Tau and src family tyrosine kinases. *Biochim. Biophys. Acta, Mol. Basis Dis.* **2005**, *1739*, 323−330.
(12) Yang, K.; Belrose, J.; Trepanier, C. H.; Lei, G.; Jackson, M. F.; MacDonald, J. F. Fyn, a potential target for Alzheimer's disease. *J. Alzheimer's Dis.* **2011**, *27*, 243−252.
(13) Lee, G.; Thangavel, R.; Sharma, V. M.; Litersky, J. M.; Bhaskar, K.; Fang, S. M.; Do, L. H.; Andreadis, A.; Van Hoesen, G.; Ksiezak-Reding, H. Phosphorylation of tau by fyn: Implications for Alzheimer's disease. *J. Neurosci.* **2004**, *24*, 2304−2312.
(14) Nygaard, H. B.; van Dyck, C. H.; Strittmatter, S. M. Fyn kinase inhibition as a novel therapy for Alzheimer's disease. *Alzheimer's Res. Ther.* **2014**, *6*, 8.
(15) Chin, J.; Palop, J. J.; Puoliväli, J.; Massaro, C.; Bien-Ly, N.; Gerstein, H.; Scearce-Levie, K.; Masliah, E.; Mucke, L. Fyn kinase induces synaptic and cognitive impairments in a transgenic mouse model of Alzheimer's disease. *J. Neurosci.* **2005**, *25*, 9694−9703.
(16) Saito, Y. D.; Jensen, A. R.; Salgia, R.; Posadas, E. M. Fyn: a novel molecular target in cancer. *Cancer* **2010**, *116*, 1629−16237.
(17) Kostic, A.; Lynch, C. D.; Sheetz, M. P. Differential matrix rigidity response in breast cancer cell lines correlates with the tissue tropism. *PLoS One* **2009**, *4*, e6361.
(18) Huang, R. Y. J.; Wang, S. M.; Hsieh, C. Y.; Wu, J. C. Lysophosphatidic. acid induces ovarian cancer cell dispersal by activating Fyn kinase associated with p120-catenin. *Int. J. Cancer* **2008**, *123*, 801−809.
(19) Posadas, E. M.; Al-Ahmadie, H.; Robinson, V. L.; Jagadeeswaran, R.; Otto, K.; Kasza, K. E.; Tretiakov, M.; Siddiqui, J.; Pienta, K. J.; Stadler, W. M.; Rinker-Schaeffer, C.; Salgia, R. FYN is overexpressed in human prostate cancer. *BJU Int.* **2009**, *103*, 171−177.
(20) Chen, Z. Y.; Cai, L.; Zhu, J.; Chen, M.; Chen, J.; Li, Z. H.; Liu, X. D.; Wang, S. G.; Bie, P.; Jiang, P.; Dong, J. H.; Li, X. W. Fyn requires HnRNPA2B1 and Sam68 to synergistically regulate apoptosis in pancreatic cancer. *Carcinogenesis* **2011**, *32*, 1419−1426.
(21) Eguchi, R.; Kubo, S.; Takeda, H.; Ohta, T.; Tabata, C.; Ogawa, H.; Nakano, T.; Fujimori, Y. Deficiency of Fyn protein is prerequisite for apoptosis induced by Src family kinase inhibitors in human mesothelioma cells. *Carcinogenesis* **2012**, *33*, 969−975.
(22) Singh, M. M.; Howard, A.; Irwin, M. E.; Gao, Y.; Lu, X.; Multani, A.; Chandra, J. Expression and activity of Fyn mediate profiferation and blastic features of chronic myelogenous leukemia. *PLoS One* **2012**, *7*, e51611.
(23) Ban, K.; Gao, Y.; Amin, H. M.; Howard, A.; Miller, C.; Lin, Q.; Leng, X.; Munsell, M.; Bar-Eli, M.; Arlinghaus, R. B.; Chandra, J. BCR-ABL1 mediates up-regulation of Fyn in chronic myelogenous leukemia. *Blood* **2008**, *111*, 2904−2908.
(24) Manetti, F.; Santucci, A.; Locatelli, G. A.; Maga, G.; Spreafico, A.; Serchi, T.; Orlandini, M.; Bernardini, G.; Caradonna, N. P.; Spallarossa, A.; Brullo, C.; Schenone, S.; Bruno, O.; Ranise, A.; Bondavalli, F.; Hoffmann, O.; Bologna, M.; Angelucci, A.; Botta, M. Identification of a novel pyrazolo[3,4-*d*]pyrimidine able to inhibit cell proliferation of a human osteogenic sarcoma in vitro and in a xenograft model in mice. *J. Med. Chem.* **2007**, *50*, 5579−5588.
(25) Manetti, F.; Brullo, C.; Magnani, M.; Mosci, F.; Chelli, B.; Crespan, E.; Schenone, S.; Naldini, A.; Bruno, O.; Trincavelli, M. L.; Maga, G.; Carraro, F.; Martini, C.; Bondavalli, F.; Botta, M. Structure-based optimization of pyrazolo[3,4-*d*]pyrimidines as Abl inhibitors and antiproliferative agents toward human leukemia cell lines. *J. Med. Chem.* **2008**, *51*, 1252−1259.
(26) Radi, M.; Tintori, C.; Musumeci, F.; Brullo, C.; Zamperini, C.; Dreassi, E.; Fallacara, A. L.; Vignaroli, G.; Crespan, E.; Zanoli, S.; Laurenzana, I.; Filippi, I.; Maga, G.; Schenone, S.; Angelucci, A.; Botta, M. Design, synthesis, and biological evaluation of pyrazolo[3,4-*d*]pyrimidines active in vivo on the Bcr-Abl T315I mutant. *J. Med. Chem.* **2013**, *56*, 5382−5394.
(27) Cozzi, M.; Giorgi, F.; Marcelli, E.; Pentimalli, F.; Forte, I. M.; Schenone, S.; D'Urso, V.; De Falco, G.; Botta, M.; Giordano, A.; Indovina, P. Antitumor activity of new pyrazolo[3,4-*d*]pyrimidine SRC kinase inhibitors in Burkitt lymphoma cell lines and its enhancement by WEE1 inhibition. *Cell Cycle* **2012**, *11*, 1029−1039.
(28) Radi, M.; Brullo, C.; Crespan, E.; Tintori, C.; Musumeci, F.; Biava, M.; Schenone, S.; Dreassi, E.; Zamperini, C.; Maga, G.; Pagano, D.; Angelucci, A.; Bologna, M.; Botta, M. Identification of potent c-Src inhibitors strongly affecting the proliferation of human neuroblastoma cells. *Bioorg. Med. Chem. Lett.* **2011**, *21*, 5928−5933.
(29) Falchi, F.; Manetti, F.; Carraro, F.; Naldini, A.; Maga, G.; Crespan, E.; Schenone, S.; Bruno, O.; Brullo, C.; Botta, M. 3D QSAR models built on structure-based alignments of Abl tyrosine kinase inhibitors. *ChemMedChem* **2009**, *6*, 976−987.
(30) Kruewel, T.; Schenone, S.; Radi, M.; Maga, G.; Rohrbeck, A.; Botta, M.; Borlak, J. Molecular characterization of c-Abl/c-Src kinase inhibitors targeted against murine tumour progenitor cells that express stem cell markers. *PLoS One* **2010**, *5*, e14143.
(31) Radi, M.; Dreassi, E.; Brullo, C.; Crespan, E.; Tintori, C.; Bernardo, V.; Valoti, M.; Zamperini, C.; Daigl, H.; Musumeci, F.; Carraro, F.; Naldini, A.; Filippi, I.; Maga, G.; Schenone, S.; Botta, M. Design, synthesis, biological activity, and ADME properties of pyrazolo[3,4-*d*]pyrimidines active in hypoxic human leukemia cells: a lead optimization study. *J. Med. Chem.* **2011**, *54*, 2610−2626.
(32) Schenone, S.; Bruno, O.; Bondavalli, F.; Ranise, A.; Mosti, L.; Menozzi, G.; Fossa, P.; Donnini, S.; Santoro, A.; Ziche, M.; Manetti, F.; Botta, M. Antiproliferative activity of new 1-aryl-4-amino-1*H*-pyrazolo[3,4-*d*]pyrimidine derivatives toward the human epidermoid carcinoma A431 cell line. *Eur. J. Med. Chem.* **2004**, *39*, 939−946.
(33) Poli, G.; Tuccinardi, T.; Rizzolio, F.; Caligiuri, I.; Botta, L.; Granchi, C.; Ortore, G.; Minutolo, F.; Schenone, S.; Martinelli, A. Identification of new Fyn kinase inhibitors using a FLAP-based approach. *J. Chem. Inf. Model.* **2013**, *53*, 2538−2547.
(34) Hanke, J. H.; Gardner, J. P.; Dow, R. L.; Changelian, P. S.; Brissette, W. H.; Weringer, E. J.; Pollok, B. A.; Connelly, P. A. Discovery of a novel, potent, and Src family-selective tyrosine kinase inhibitor. Study of Lck- and FynT-dependent T cell activation. *J. Biol. Chem.* **1996**, *271*, 695−701.
(35) Schindler, T.; Sicheri, F.; Pico, A.; Gazit, A.; Levitzki, A.; Kuriyan, J. Crystal structure of Hck in complex with a Src family-selective tyrosine kinase inhibitor. *Mol. Cell* **1999**, *3*, 639−648.

DOI: 10.1021/acs.jmedchem.5b00140
J. Med. Chem. 2015, 58, 4590−4609

(36) Zhu, X.; Kim, J. L.; Newcomb, J. R.; Rose, P. E.; Stover, D. R.; Toledo, L. M.; Zhao, H.; Morgenstern, K. A. Structural analysis of the lymphocyte-specific kinase Lck in complex with non-selective and Src family selective kinase inhibitors. *Structure* **1999**, *7*, 651−661.
(37) Vignaroli, G.; Mencarelli, M.; Sementa, D.; Crespan, E.; Kissova, M.; Maga, G.; Schenone, S.; Radi, M.; Botta, M. Exploring the chemical space around the privileged pyrazolo[3,4-*d*]pyrimidine scaffold: toward novel allosteric inhibitors of T315I-mutated Abl. *ACS Comb. Sci.* **2014**, *16*, 168−175.
(38) Schenone, S.; Bruno, O.; Bondavalli, F.; Ranise, A.; Mosti, L.; Menozzi, G.; Fossa, P.; Manetti, F.; Morbidelli, L.; Trincavelli, L.; Martini, C.; Lucacchini, A. Synthesis of 1-(2-chloro-2-phenylethyl)-6-methylthio-1*H*-pyrazolo[3,4-*d*]pyrimidines 4-amino substituted and their biological evaluation. *Eur. J. Med. Chem.* **2004**, *39*, 153−160.
(39) Benoit, G. Hydroxyalkyl hydrazines. *Bull. Soc. Chim. Fr.* **1939**, *6*, 708−715.
(40) Bruno, O.; Brullo, C.; Bondavalli, F.; Ranise, A.; Schenone, S.; Falzarano, M. S.; Varani, K.; Spisani, S. 2-Phenyl-2,3-dihydro-1*H*-imidazo[1,2-*b*]pyrazole derivatives: new potent inhibitors of fMLP-induced neutrophil chemotaxis. *Bioorg. Med. Chem. Lett.* **2007**, *17*, 3696−3701.
(41) Hanefeld, U.; Rees, C. W.; White, A. J. P.; Williams, D. J. One-pot synthesis of tetrasubstituted pyrazoles-proof of regiochemistry. *J. Chem.Soc., Perkin Trans. 1* **1996**, *13*, 1545−1552.
(42) Robins, R. K. Potential purine antagonists. I. Synthesis of some 4,6-substituted pyrazolo[3,4-*d*]pyrimidines. *J. Am. Chem. Soc.* **1956**, *78*, 784−790.
(43) Hirst, G. C.; Calderwood, D.; Wishart, N.; Rafferty, P.; Ritter, K.; Arnold, L. D.; Friedman, M. M. Preparation of pyrazolopyrimidines as protein kinase inhibitors. PCT Int. Appl. WO 2001019829 A2 20010322, (2001).
(44) Medina, M.; Avila, J. New insights into the role of glycogen synthase kinase-3 in Alzheimer's disease. *Expert Opin. Ther. Targets* **2014**, *18*, 69−77.
(45) Smith, B.; Medda, F.; Gokhale, V.; Dunckley, T.; Hulme, C. Recent advances in the design, synthesis, and biological evaluation of selective DYRK1A inhibitors: a new avenue for a disease modifying treatment of Alzheimer's? *ACS Chem. Neurosci.* **2012**, *3*, 857−872.
(46) Agholme, L.; Lindström, T.; Kågedal, K.; Marcusson, J.; Hallbeck, M. An in vitro model for neuroscience: differentiation of SH-SY5Y cells into cells with morphological and biochemical characteristics of mature neurons. *J. Alzheimer's Dis* **2010**, *20*, 1069−1082.
(47) Ryan, D. A.; Narrow, W. C.; Federoff, H. J.; Bowers, W. J. An improved method for generating consistent soluble amyloid-beta oligomer preparations for in vitro neurotoxicity studies. *J. Neurosci. Methods* **2010**, *190*, 171−179.
(48) Wong, J.; Higgins, M.; Halliday, G.; Garner, B. Amyloid beta selectively modulates neuronal TrkB alternative transcript expression with implications for Alzheimer's disease. *Neuroscience* **2012**, *210*, 363−374.
(49) Zamperini, C.; Dreassi, E.; Vignaroli, G.; Radi, M.; Dragoni, S.; Schenone, S.; Musumeci, F.; Valoti, M.; Antiochia, R.; Botta, M. CYP-dependent metabolism of antitumor pyrazolo[3,4-*d*]pyrimidine derivatives is characterized by an oxidative dechlorination reaction. *Drug Metab. Pharmacokinet.* **2014**, *29*, 433−440.
(50) Kinoshita, T.; Matsubara, M.; Ishiguro, H.; Okita, K.; Tada, T. Structure of human Fyn kinase domain complexed with staurosporine. *Biochem. Biophys. Res. Commun.* **2006**, *346*, 840−844.
(51) *Maestro*, version 9.2; Schrödinger, LLC: New York, 2011.
(52) *LigPrep*, version 2.5; Schrödinger, LLC: New York, 2011.
(53) Irwin, J. J.; Shoichet, B. K. ZINC—A free database of commercially available compounds for virtual screening. *J. Chem. Inf. Model.* **2005**, *45*, 177−182.
(54) Verdonk, M. L.; Cole, J. C.; Hartshorn, M. J.; Murray, C. W.; Taylor, R. D. Improved protein−ligand docking using GOLD. *Proteins* **2003**, *52*, 609−623.
(55) Williams, N. K.; Lucet, I. S.; Klinken, S. P.; Ingley, E.; Rossjohn, J. Crystal structures of the Lyn protein tyrosine kinase domain in its Apo- and inhibitor-bound state. *J. Biol. Chem.* **2009**, *284*, 284−291.
(56) Zhu, X.; Kim, J. L.; Newcomb, J. R.; Rose, P. E.; Stover, D. R.; Toledo, L. M.; Zhao, H.; Morgenstern, K. A. Structural analysis of the lymphocyte-specific kinase Lck in complex with non-selective and Src family selective kinase inhibitors. *Structure* **1999**, *7*, 651−661.
(57) Case, D. A.; Darden, T. A.; Cheatham, T. E., III; Simmerling, C. L.; Wang, J.; Duke, R. E.; Luo, R.; Walker, R. C.; Zhang, W.; Merz, K. M.; Roberts, B.; Wang, B.; Hayik, S.; Roitberg, A.; Seabra, G.; Kolossvai, I.; Wong, K. F.; Paesani, F.; Vanicek, J.; Liu, J.; Wu, X.; Brozell, S. R.; Steinbrecher, T.; Gohlke, H.; Cai, Q.; Ye, X.; Wang, J.; Hsieh, M.-J.; Cui, G.; Roe, D. R.; Mathews, D. H.; Seetin, M. G.; Sagui, C.; Babin, V.; Luchko, T.; Gusarov, S.; Kovalenko, A.; Kollman, P. A.*AMBER 11*; University of California: San Francisco, 2010.
(58) Wang, J.; Wolf, R. M.; Caldwell, J. W.; Kollman, P. A.; Case, D. A. Development and testing of a general amber force field. *J. Comput. Chem.* **2004**, *25*, 1157−1174.
(59) Jakalian, A.; Jack, D. B.; Bayly, C. I. Fast, efficient generation of high-quality atomic charges. AM1-BCC model: II. Parameterization and validation. *J. Comput. Chem.* **2002**, *23*, 1623−1641.
(60) Homeyer, N.; Horn, A. H.; Lanig, H.; Sticht, H. AMBER force-field parameters for phosphorylated amino acids in different protonation states: phosphoserine, phosphothreonine, phosphotyrosine, and phosphohistidine. *J. Mol. Model.* **2006**, *12*, 281−289.
(61) Ryckaert, J. P.; Ciccotti, G.; Berendsen, H. J. C. Numerical integration of the cartesian equations of motion of a system with constraints: molecular dynamics of *n*-alkanes. *J. Comput. Phys.* **1977**, *23*, 327−341.
(62) Kottalam, J.; Case, D. A. Langevin modes of macromolecules: applications to crambin and DNA hexamers. *Biopolymers* **1990**, *29*, 1409−1421.
(63) Loncharich, R. J.; Brooks, B. R.; Pastor, R. W. Langevin dynamics of peptides: the frictional dependence of isomerization rates of *N*-acetylalanyl-*N*′-methylamide. *Biopolymers* **1992**, *32*, 523−535.
(64) Tintori, C.; Fallacara, A. L.; Radi, M.; Zamperini, C.; Dreassi, E.; Crespan, E.; Maga, G.; Schenone, S.; Musumeci, F.; Brullo, C.; Richters, A.; Gasparrini, F.; Angelucci, A.; Festuccia, C.; Delle Monache, S.; Rauh, D.; Botta, M. Combining X-ray crystallography and molecular modeling toward the optimization of pyrazolo[3,4-*d*]pyrimidines as potent c-Src inhibitors active in vivo against neuroblastoma. *J. Med. Chem.* **2015**, *58*, 347−361.
(65) Carraro, F.; Naldini, A.; Pucci, A.; Locatelli, G. A.; Maga, G.; Schenone, S.; Bruno, O.; Ranise, A.; Bondavalli, F.; Brullo, C.; Fossa, P.; Menozzi, G.; Mosti, L.; Modugno, M.; Tintori, C.; Manetti, F.; Botta, M. Pyrazolo[3,4-*d*]pyrimidines as potent antiproliferative and proapoptotic agents toward A431 and 8701-BC cells in culture via inhibition of c-Src phosphorylation. *J. Med. Chem.* **2006**, *49*, 1549−1561.
(66) Falco, E. A.; Hitchings, G. H. Studies on condensed pyrimidine Systems. XV. Some Pyrazolo[3,4-*d*]pyrimidines. *J. Am. Chem. Soc.* **1956**, *78*, 3143−3145.
(67) Abassi, Y. A.; Xi, B.; Zhang, W.; Ye, P.; Kirstein, S. L.; Gaylord, M. R.; Feinstein, S. C.; Wang, X.; Xu, X. Kinetic cell-based morphological screening: prediction of mechanism of compound action and off-target effects. *Chem. Biol.* **2009**, *16*, 712−723.
(68) Wohnsland, F.; Faller, B. High-throughput permeability pH profile and high-throughput alkane/water log *P* with artificial membranes. *J. Med. Chem.* **2001**, *44*, 923−930.
(69) Sugano, K.; Hamada, H.; Machida, M.; Ushio, H. High throughput prediction of oral absorption: improvement of the composition of the lipid solution used in parallel artificial membrane permeation assay. *J. Biomol. Screening* **2001**, *6*, 189−196.

DOI: 10.1021/acs.jmedchem.5b00140
J. Med. Chem. 2015, 58, 4590−4609